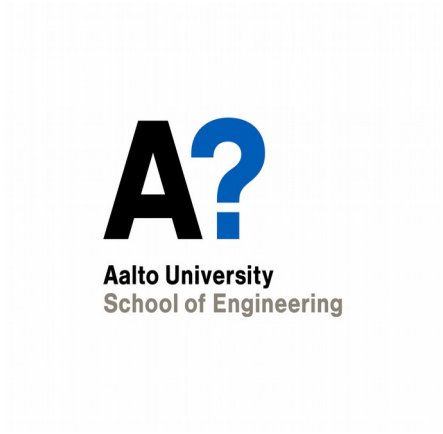

Mikko Köykkä

Modeling of ship structure-borne underwater radiated noise

Thesis submitted for examination for the degree of Master of Science in Technology

Espoo 07.04.2016
Thesis supervisor: Asst. Prof. Jani Romanoff
Thesis advisor: Lic.Sc. (Tech.) Martti Helamaa
Thesis advisor: M.Sc. (Tech.) Roope Kotiranta

Aalto-yliopisto
Insinööritieteiden korkeakoulu

Aalto-yliopisto, PL 11000, 00076 AALTO
www.aalto.fi
Diplomityön tiivistelmä

Tekijä Mikko Köykkä.

Työn nimi Aluksen veteen välittyvän runkoäänen mallinnus

Koulutusohjelma Konetekniikan koulusohjelma

Pää-/sivuaine Lentotekniikka/ teknillinen mekaniikka **Koodi** Kul-34

Työn valvoja Jani Romanoff

Työn ohjaaja(t) Martti Helamaa, Roope Kotiranta

Päivämäärä 07.04.2016 **Sivumäärä** 67 **Kieli** Englanti

Perinteisesti sota- ja erikoisalusten suunnittelussa on kiinnitetty huomiota aluksen runkomelun hallintaan ja mallintamiseen. Lisääntynyt tietoisuus alusliikenteen ympäristökuormasta on luonut myös kaupallista laivaustoimintaa harjoittavien yritysten parissa kiinnostusta runkomelun mallintamiseen. Aluksen koneistossa syntyvä runkoääni välittyy kiinteiden aineiden, nesteiden sekä kaasujen värähtelynä veteen ja ilmaan.

Tämä työ tarkastelee runkoäänen mallintamiseen käytettyjä laskentamenetelmiä. Laskennallisten menetelmien vahvistamiseksi työssä suoritetaan merikoe runkoäänen mittaamiseksi käyttäen pientä referenssirakennetta. Referenssirakenteen käyttö luo hallittavan ympäristön vertailun suorittamiseksi. Työssä käytetään kaupallista ohjelmaa laskemaan voimaimpulssin siirtyminen laivan rakennetta pitkin. Laskenta tehdään käyttämällä elementtimentelmää ja tilastollista energia-analyysiä. Lisäksi tuloksia verrataan analyyttisillä kaavoilla laskettuihin palkin ja levyn ominaistaajuuksiin.

Työssä mitatut ja laskennalliset ominaistaajuudet vastaavat toisiaan. Mitatut värähtelyn ominaisuudet vastaavat kirjallisuudessa esitettyjä ominaisuuksia. Elementtimenetelmällä ja tilastollisella energia-analyysillä laskettujen siirtymien havaittiin vastaavan mitattuja tuloksia. Elementtimenetelmä on laskennallisesti raskas ja rakenteesta vaaditaan tarkka malli. Käytetty veden mallinntamismentelmä havaittiin yhdessä elementtimentelmän kanssa käytettynä epätarkaksi. Tilastollinen energia-analyysi on laskennallisesti kevyt, sekä sillä laskettu rakenteen värähtely pystyi ennustamaan matalillakin taajuuksilla värähtelyn kohtalaisen tarkasti.

Työssä keskityttiin pieneen referenssirakenteeseen matalilla taajuuksilla. Validointi pitää suorittaa myös isommalla rakenteella ja korkeammilla taajuuksilla.

Avainsanat Runkoääni, elementtimenetelmä, tilastollinen energia-analyysi, koneisto, alus, mittaus

Aalto University
School of Engineering

Aalto University, P.O. BOX 11000, 00076
AALTO
www.aalto.fi
Abstract of master's thesis

Author Mikko Köykkä

Title of thesis Modeling of ship structure-borne underwater radiated noise

Degree programme Degree programme in Mechanical Engineering

Major/minor Aeronautical Engineering/ Tecnical mechanics **Code** Kul-34

Thesis supervisor Jani Romanoff

Thesis advisor(s) Martti Helamaa, Roope Kotiranta

Date 07.04.2016 **Number of pages** 67 **Language** English

Increased environmental awareness has created the need in commercial shipping, in addition to established military requirements, to understand and manage structure-borne machinery noise radiated to water. Noise created from machinery is transferred via vibrations in solids and fluids. These vibrations have different characteristics in low and high frequency range, resulting the need of different calculating methods.

The objective of this thesis is to validate main calculating methods used in the modeling of structure-borne sound against measurements. Sea trials are carried out with a small reference model structure to model transfer of impulse shock from source to water in controlled environment. Commercial structure-borne sound modeling software is used to model response of the structure to the shock impulse using finite element method and statistical energy analysis. Also analytical equations are used to calculate response simplified of beam and plate.

Natural frequencies measured in this thesis correspond to the calculated natural frequencies. Measured modal properties follow pattern established in the literature. Forced response calculated using finite element method and statistical energy analysis were found to correspond to measurements. Finite element method provided accurate results. Method used to model effect of water loading in finite element analysis was found to be inaccurate. Finite element method was found to have high computational cost. Also required level of structural detail was high. Statistical energy analysis is computationally light and capable to predict response at lower frequencies with relative accuracy.

In this work, the study is focused on vibrational velocity levels on a small reference structure in low frequencies. Further validation is required on a larger structure and in high frequencies.

Keywords Strcture borne sound, finite element method, statistical energy analysis, machinery, ship, measurement

Foreword

In addition to traditional noise management requirements of military and special vessels, the increased environmental awareness has created demand to understand and manage structure-borne noise. This thesis prepares to integration of structure-borne noise in to ship design by studying and validating main modeling tools. This work is a part of Smulan 2 TP5 Underwater Acoustic research project, funded by the Finnish Funding Agency for Innovation, TEKES.

First I would like to thank my advisers Martti Helamaa and Roope Kotiranta for words of advice, support and for introducing me to marine environment. I am grateful for my supervising professor Jani Romanoff, who has provided excellent guidance and valuable comments to complete this thesis. I wish to thank emeritus professor Olli Saarela for helping me to start this thesis.

I wold like to thank TEKES for providing funding to my thesis.

All employees of Surma have supported me while I worked with my the thesis. My thanks goes to everyone for helping me. I wold like to thank Jukka Pajala of Finish Environment Institute for providing *Aranda* measurements and other support. I had a great day at sea with the Antti Lindfors and Toni Meriläinen of Luode Consulting, conducting the measurements. Thank you and the whole crew for the day.

I would like to thank ESI Group for providing me software to use in my thesis and all of the employees of ESI Group I worked with to complete my thesis. You also arranged me the great opportunity to to present results of this work and meet international experts of this field at Marine SIG 2016 in Southampton UK.

I would like to give a special thanks Arthur Henry of ESI Group for teaching me the basics of modeling of structure-borne sound in August 2015 in Munich. You also patiently supported me while I was creating models of my own for this thesis. Our discussions and your instructions have helped greatly to shape my thesis.

A special and warm compliments to my family and friends for helping me while studying at the university.

Above all, the greatest compliments is reserved for the most amazing and wonderful person, who took me as her husband, Jenny. Your love and support have carried me through university. This would not happened without you.

Espoo 07.04.2016

Mikko Köykkä

Table of Contents

List of abbreviations

1D	One dimensional
2D	Two dimensional
FE	Finite Element
CSV	Comma Separated Value
FEM	Finite Element Method
N/A	Not Applicable
SEA	Statistical Energy Analysis
SIF	Semi Infinite Fluid
UTC	Coordinated Universal Time

Symbols

A	Area
a	Acceleration
$\boldsymbol{C}$	Damping matrix
C	Damping coefficient
c_p	Phase velocity
c	Velocity of sound in fluid
$\tilde{\boldsymbol{C}}$	Energy coupling matrix
c_g	Group velocity
$\boldsymbol{D}$	Global acoustic damping
D_{mm}	Stiffness matrix of wavelet method
D_e	Bending stiffness of plate
$d_{element}$	Mesh density factor
E	Elastic modulus
E_j	Energy of subsystem j
$\boldsymbol{E}$	Energy vector
F	Force
f	Frequency
f_n	Natural frequency
G	Shear modulus
g	g-force
$\boldsymbol{H}$	Global acoustic stiffness
h	Plate thickness
I	Area moment
j	Imaginary unit
K	Stiffness constant
$\boldsymbol{K}$	Stiffness matrix
k	Wave number
$\boldsymbol{L}$	Global structural-acoustic coupling matrix
L	Length
$\boldsymbol{M}$	Mass matrix
M	Mass

M_A	Lewis' approximation of added mass
m	Distributed mass
$\tilde{M}$	Mole
N	Mode count
n	Modal density
P	Power
p	pressure
$\boldsymbol{Q}$	Global acoustic inertia
r	Radius
t	Time
V	Volume
X	Amplitude
α_k	Dimensionless wave number, x direction
β_k	Dimensionless wave number, y direction
γ	Heat capacity ratio
ε	Strain
η	Damping loss factor
η_{jk}	Coupling loss factor between systems j and k
λ	Wave length
ν	Poisson’s ratio
η	Coupling loss factor
ξ	Critical dampening
ρ	Density
σ_{rad}	Radiation loss factor
τ	Transmission loss coefficient
Φ	Phase
φ	Shape function
ω	Angular frequency
ω_n	Angular natural frequency

1 Introduction

1.1 Background

> "Machinery signatures?"
> "They're running at very low power settings skipper, not enough for a classification. I got steam noises on all three, that makes 'em nucs but if you look here you can see that we're just not getting enough signal for anything else."
> . . .
> "Captain, classify the target at two-eight-zero as an Alfa-class!"
> "You sure?"
> "Yes sir. That is an Alfa type engine plant. I have clearly it now."
> "Set it up! We'll run one fish in deep, dogleg it at slow speed then pop it up right underneath him."
> . . .
> The Alfa might hear the air blast or he might not, McCaffertry knew. The torpedo moved off at forty knots on heading of three five-zero, well of the bearing to target
>
> (Clancy, 1987, pp. 614–615)

This is how submarines of rivaling navies might have fought over the control of the oceans in the mid 1980s, told by Tom Clancy in his novel *Red Storm Rising*. Although this encounter deep in the ocean is fictional, it shows the importance of understanding and managing underwater noise, radiating from machinery, to survive and fight efficiently in armed conflict. The importance of noise management has been increased from the first submarine battles of the First World War. Clearly, noise makes warships more vulnerable to attack and decreases combat effectiveness. (Ross, 1987, chap. 1)

Outside of the military, only underwater noise of the research vessels and fishing boats has been in concern. In recent years there has been increased awareness of the effect of underwater noise to marine mammals. Corporations are currently profiling on environmental issues, leading to growing interest in commercial shipping industry to management underwater noise profile of ship, among other environmental improvements. In 2014, the International Maritime Organization published first set of guidelines to protect marine life from underwater noise created by commercial shipping in 2014 (International Maritime Organization, 2014). Emerging environmental threats arise in the arctic regions, where shipping is becoming possible in previously untouched areas. This new noise source exposes previously untouched marine life in narrow corridors to noise (Protection of the Arctic Marine Environment Working Group, 2009).

In ship design, the goal to optimize fuel efficiency has led to using lightweight structures, slow running main engines, and high propulsion power. To reduce interior space, accommodation spaces are placed close to the machinery. (Bertram, 2011, chap. 5.1)

Traditionally, the problems involving structure-borne sound has been solved using simplifying analytical and empirical methods. Advances in computer aided engineering have made it possible to model complex problems of structure-borne sound more accurately. Computer aided engineering includes tools to create drawings and product models tools to study dynamical behavior of the structure and environment. The availability of scripted automation in engineering programs have made modeling process easier, allowing use of numerical tools earlier at the design process to variate parameters of the design. Increases in the computer resources have made solving more complex problems possible. In modern engineering, software provides important tools for engineering, simplifying the design and analysis process. (Ross, 1987, chap. 1; Fahy and Gardonio, 2007, chap. 8.1; Henry, 2015)

In designing quieter ships, there is a need to understand and simulate noise generated by operating the ship. According to the second law of thermodynamics, noise is inevitable in all mechanical processes as heat can not be converted perfectly to work. Equally, no mechanical process is viable without generating vibration experienced as noise. (Ross, 1987, p. 1; Bertram, 2011, chap. 5.1; Mansfield and O'Sullivan, 2011, chap. 11.4; Lloyd's Register, 2015, chap. 1.2).

Any disturbance, including sound, is carried in elastic mediums as a wave motion that causes vibration. By studying transfer path, it is possible to estimate the location for the installation of the most effective noise control treatments from source to water. In the end of the transfer path, vibrational velocities are calculated to determinate sound levels. (Fahy, 2000, p. 7; Henry, 2015)

The characteristics of vibration divide the frequency range into three separate regions: low frequency, mid frequency, and high frequency range. Each of these ranges has different behavioral characteristics and requirements for analysis. In low frequencies, the response exhibits strong modal behavior, indicated by isolated response peaks. This usually occurs at the first natural frequencies. In low frequencies, the structural vibration is approximated analytically as a nonuniform beam. In high frequencies, the modal density is high, indicated by a smooth response spectra. The boundary conditions, the material properties and the geometry of the structure are not important in the high frequencies. For analytical analysis in high frequencies, excitation force is assumed to cause only small area to vibrate, while remaining of the structure is considered as an infinitive sound barrier, an infinite baffle. Thus, plate theory is used to model response in high frequencies analytically. In mid frequencies the modal density is not constant and the response spectra exhibits local highs and lows. In the mid frequency range the model is sensitive to boundary conditions, material properties and geometry. (Ross, 1987, chap. 4.11; Soize, Desanti and David, 1992, chap. 2.5; Rabbiolo, Bernhard and Milner, 2004, chap. 1)

Typical marine vessel is a complicated structure, vibrating at a wide frequency range. Consequently, the ship hull radiates sound over a wide frequency range. The frequency

range is relative to the properties of studied structure and fluid. Illustration of relative frequency ranges is presented on the figure 1. (Ross, 1987, chap. 4.11)

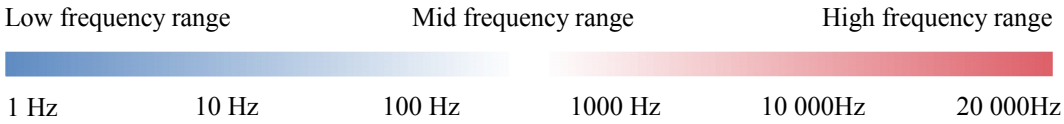

Figure 1: Division of frequency range with respect to sound. (Modified from Cicirello et al., 2012)

Waves have dual modal characteristics; the waves are divided to coherent and incoherent parts. Coherent direct field vibration is the first impulse to the system. There is no variance in the first impulse, thus it is readily calculated using any deterministic methods. Incoherent reverberant field is created from interactions at the boundaries of the system and blocked connections. When boundary is not perfectly regular, coherence of a direct field is lost over time. When the behavior of waves is completely incoherent, the reverberant field is said to be diffused. This diffused reverberant field is solved using statical energy analysis. The effect of reverberant field is small in lower frequencies, so the deterministic methods are suitable to model the response of the structure. As the frequency increases, the reverberant field dominates the vibration In high frequencies, the vibration field is more random and small imperfections of a structure dominate the solution. The two different field types are illustrated in figure 2. (Lyon and DeJong, 1994, pp. 19, 39–40, 44–47)

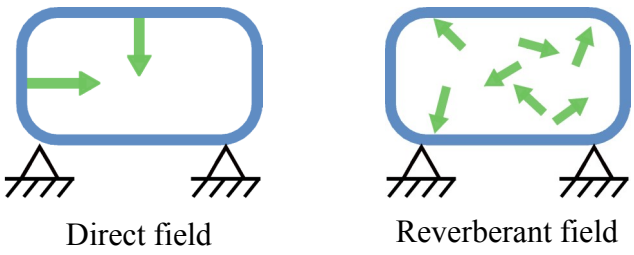

Figure 2: Direct and reverberant vibrational field.

The type of vibrational field is not the only selection criteria, also the type of the problem, the phase of the design, and required results needs to be considered. Deterministic methods are useful in predicting vibrational levels in a specified location. Analytical solutions are only available on simple structures. The classical numerical methods used to model more complex structures are computationally heavy and very

detailed structure is needed for accurate response in the high frequencies. To model structure vibrations at higher frequencies and with fewer structural details, statistical methods are developed. (Henry, 2015)

Noise proceeds from machinery or other sources to water and air in three steps, presented in figure 3. Impulse created by the machinery or any other mechanism is transferred via structure and air to vibration of plates in contact with water. In this work, the initial impulse is measured and vibration of plates in contact with water is measured and calculated using the main modeling methods of structure-borne sound. (Ross, 1987, chap. 1.1)

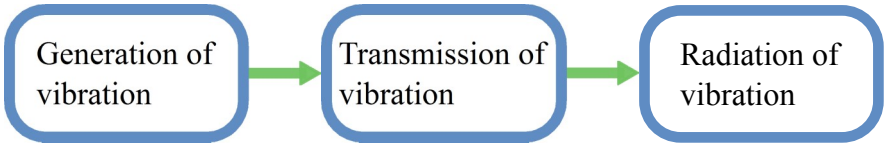

Figure 3: Division of noise production process.

This thesis is a part of Smulan 2 TP5 Underwater Acoustic research project. The project aims to develop knowledge in managing underwater noise. Noise control is required in the design process due the new environmental norms on marine traffic and requirements of special ships. New requirements demand new machinery and noise control treatments solutions to meet norms and operational demands. This Smulan project is divided into reducing noise from machinery, hydro acoustic measuring technologies and modeling methods. This thesis will start a research for establishing and validating structural acoustics modeling methods in marine industry. The final goal of the research program is to transfer ship product model from a ship design software to structure-borne sound modeling software and use the transferred model and to validate calculating methods for predicting radiated underwater noise. Modeling results will be compared to measurements conducted using research vessel *Aranda*. In this work, the main modeling tools used in analysis of structure-borne sound are identified. Results provided by the modeling tools are studied and compared to measurements to establish suitable research method and tools for analysis of *Aranda*.

1.2 Research problem

Most of the studies of underwater noise has been mainly conducted by the military. The sensitive nature of acoustic signature limits the public availability of the studies of structure-borne sound of ship radiated to underwater noise. Especially the availability of studies where calculations and measurements were compared, is limited. Recent advances in the modeling of structure-borne sound have made it possible to model ship behavior in wide frequency range. Due to increased environmental awareness, there is a growing demand for to understanding the noise signature, including sound radiated from ship to underwater noise in all ships, not only in special purpose vessels.

In this work the main tools for modeling of structure-borne noise in a marine application are studied using a small reference structure, with and without water loading. Small structure and known excitation instead of real engine load creates more controlled environment to validate calculation methods. The results from main modeling methods, statistical energy analysis and finite element method, are validated against measurements. Results from statistical energy analysis is validated directly against measurement of forced response. Results from finite element analysis are validated in two parts: modal response of finite element model is compared to measured natural frequencies to validate the model. Calculation of forced response of finite element model is validated against measured forced response. Modal response is calculated also using analytical beam and plate theory. Water loading is modeled using wavelet method, a recent development derived from Rayleigh integral, used to analyze sound radiated by a vibrating planar body. This method is not as accurate as element based methods, as it does not model radiation from water to structure. In finite element analysis, wavelet method is only available at calculating modal response, not in calculating forced response. Based on literature, effect on results from using wavelet method instead of element method were estimated to be low, while computational cost is lighter compared to element based methods. (Langley, 2007; Blanchet and Caillet, 2012)

The reference structure is modeled using a commercial computer aided engineering tool, VA One and analytical beam and plate equations. Vibrational response of the structure is estimated using statistical energy analysis and finite element method. Water loading is modeled using wavelet method. Sea trials for the reference structure are planned and conducted to obtain a baseline for validation of the calculating methods. The response of the reference structure to a known excitation is measured on water loaded condition and response is measured. The excitation is simulating loading of machinery. Measured vibrational velocities are compared to calculated response velocities and calculated modal behavior of the reference structure.

1.3 Objective and limitations

The objective of this thesis is to validate the main modeling methods used to predict structure-borne sound. Studied vibration is structure-borne noise radiating from the machinery to underwater noise. The modeling methods are validated against measurements, on a small scale reference structure. To complete the objective, sea trials are conducted on a reference structure to gather validation data. The main calculating methods are used to create structure-borne sound models of the reference structure under same conditions as in the sea trials.

The studied frequency range is limited to frequency range of a typical diesel marine engine, below 1000 Hz. In addition to the main engines, this frequency range includes auxiliary machinery and gears of ship power line. Noise sources, including various structural and hydrodynamic components, in addition to power line are presented on figure 4.

The range includes elements of typical higher frequency range, allowing simultaneous study of both main calculation methods, finite element method and statistical energy analysis. Low end of this frequency range is sufficiently low for analytical beam and plate theory to be used.. (Collier, 1997)

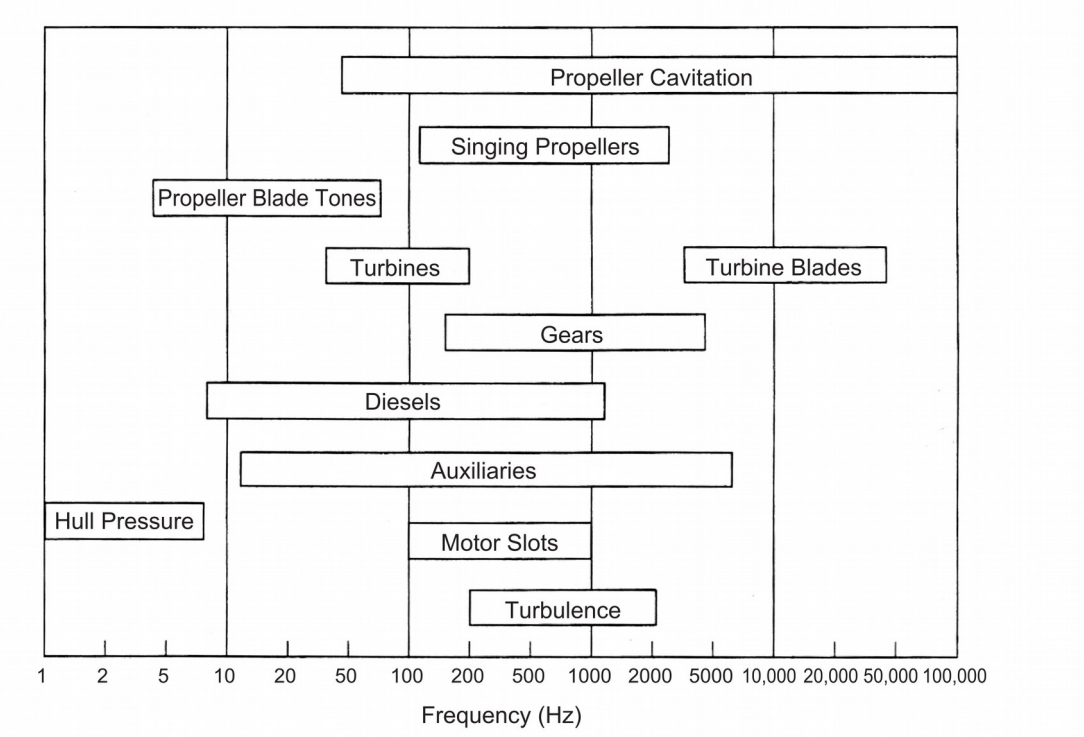

Figure 4: Noise sources of ship with corresponding frequency ranges. (Fischer and Collier, 2007, p. 1220)

Comprehensive measurements on ship underwater noise conducted in 1940s, quoted by Ross (1987), demonstrate dominance of low and mid frequency frequency region in vibrational spectrum levels. At nine knots, the noise from machinery is the dominate source, as speed increases the sound spectrum level also increases significantly. In high speeds the propeller cavitation in high dominates noise profile as presented on figure 5. Dominance of propeller noise at high speeds suppresses any effect of noise control treatment in transfer path from machinery to water. In lower speeds, usually used when operational profile requires quiet operation, the propeller does not cavitate. Thus cavitation noise from propeller is excluded from the study. (Ross, 1987, p. 8.6; Fischer and Collier, 2007; Bertram, 2011, p. 2.6)

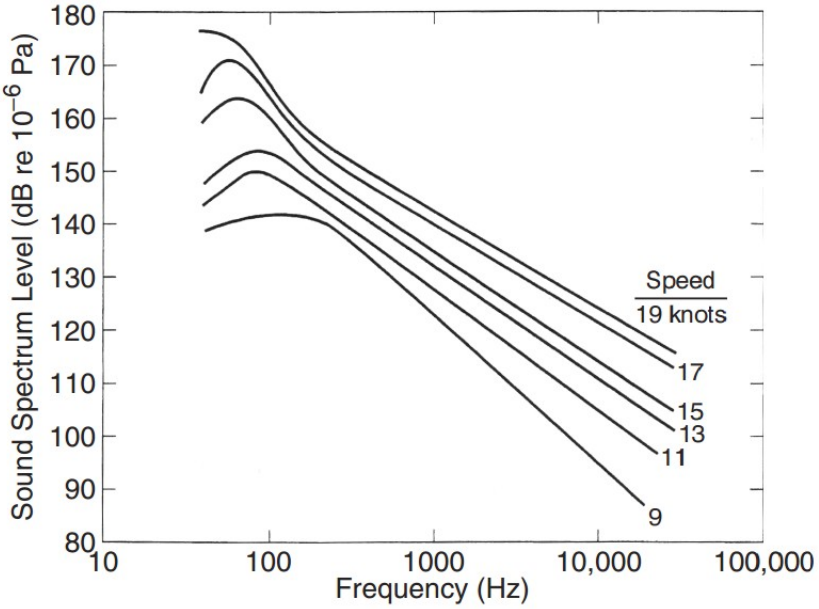

Figure 5: Radiated underwater noise levels of passenger ship Astrid. (U.S. Office of Scientific R&D 1960 as presented by Ross, 1987, p. 275. The figure from Fischer and Collier, 2007, p. 2007)

2 Literature review

The calculating methods used to model structure-borne noise are introduced in literature review before proceeding to theory of structure-borne sound. After the review of literature of the main calculating methods, a brief introduction of research conducted on other calculating methods is presented to provide an overview on emerging calculating methods and development on mid frequency range analysis.

A classical introduction to underwater noise was written by Ross (1987). Part of his work was based on work started by Cremer during the World War II and most recently published in the book *Structure-borne sound: structural vibrations and sound radiation at audio frequencies (2005)*. Ross also reproduces comprehensive studies to ship underwater acoustics, conducted in 1940s. Advances in other calculating methods are introduced in doctoral theses by Desmet (1998) and Caresta (2009). Desmet reviews practicality studies of various forms of coupled acoustic-structure analysis in his doctoral thesis of wave based method. Caresta introduces various studies of structural response of shells and sound radiated from vibrating bodies. Lucas (2008) and Pluymers (2006) reviewed in their respective doctoral theses on various hybrid methods used to solve structure-borne sound problems in mid frequency range. Lamula (2015) reported measurements made on board *Aranda* when the ship was at harbor and with engines and auxiliary equipment shut down. Below 250 Hz measured response did not have sufficient quality when used source was shock impulse. For vibrating impulse, quality results begun from 800 Hz.

Plunt (1980a, 1980b) concluded in his thesis that statistical energy analysis is applicable to model structure-borne sound in ships. Results were found to agree with the measurements in higher frequencies. The comparison of measurements and statistical energy analysis calculations also demonstrate the need for use of different methods to analyze the lower frequencies as statistical energy analysis does not predict variation in velocity level in those frequencies. The results demonstrates the fundamental properties of statistical energy analysis. The prediction calculated using statistical energy analysis follows the general trend of the measurements while failing to predict peaks. The results also visualize how the outcome obtained using statistical energy analysis approach measurements as frequency increases.

Lu et al. (1982) compared finite element method, statistical energy analysis, and experimental results for a broadband vibrations to provide understanding in modeling machine borne vibration of ships. The test specimen consist of plates in similar shape to ship hull. In the low frequencies finite element method provided results close to those measured. Statistical energy analysis provided averaged results at the range of the greatest response. As frequency was increased, accuracy of single finite element method reduced dramatically, but using Monte Carlo analysis, the frequency range available to finite element analysis was extended to 1000 Hz. The statistical energy analysis become more accurate when frequency was increased, proving results slightly larger than measured. Lu et al. studied structural vibrations in marine applications, but no mention was made of the effect of water loading.

Tratch (1985) studied structure-borne noise in a section of a ship hull in his thesis. Vibrations were calculated using statistical energy analysis and were compared to experimental results of a small scale section of the hull. Thatch's study did not include coupling factor for hull-water interaction. The results from statistical energy analysis show good correspondence with experimental results. The outcome also demonstrated the need to include both bending and in-plane waves.

Cushieri and Sun (1994) studied modeling of engine foundation using statistical energy analysis. Previous studies have found modeling engine foundation, especially determining coupling loss factor and internal loss factor difficult. In this work, coupling loss factors were estimated using measured mobility data, obtained by measuring mobility function of each part of disassembled bearing of foundation. Internal loss factors were measured using time decay method and power input methods. Response calculated using statistical energy analysis was compared to measured response. The calculated response was found to agree with the measurements.

Hynnä et al. (1995) developed a method to create statistical energy analysis model for a complex ship. Statistical energy analysis model of three different types of ship were created. The method was used to predict noise levels inside the ship. Predictions made by statistical energy analysis were compared against measurements. Statistical energy analysis was found to provide results close to measured sound level. The studied frequency range extended from 63 Hz to 8 kHz. In the lowest frequency band the difference between measurements and calculations were found out to be 2 dB larger.

Homm et al. (2003) studied a coupled finite element–boundary element system in a model of submerged cylindrical shell to analytical solution of the model and experiments. Increase of details in the model did provide more accurate results but inaccuracies in boundary conditions prohibit use of overly detailed model. Homm et al. conclude modeling of structure and formulation of boundary conditions to be the most critical factors in simulating vibrational behavior of structures.

Brunner et al. (2008) studied applicability of coupled finite element–boundary element model in frequency range from 0.5 Hz to 100 Hz. The structure used in the study was a submerged 20 m long cylinder. With the right optimization of computational method calculation time was found to be acceptable. A further study by Brunner et al. (2009) focused on combined finite element–boundary element model in simulation of behavior of a ships structure. They compared two methods to model effects of water surface, mixed formulation to discrete water surface only near the ship and half-space fundamental solution. Frequencies studied were in range from 0.5Hz to 25 Hz.

Lin et al. (2009) studied modeling of ship engine foundations using finite element method. Out of plane input mobilities of the engine bed calculated using infinite beam were found to be close to overall level of input mobilities calculated using finite model. This indicates the input mobility is controlled by stiffness of engine bed. Damping effect of plates in ship decks and hull was found to effect only propagation of long wavelength vibration. First estimates on wave propagation are suggested to performed using only major stiffened beams of ship structure. Lin et al. observe that excitations

from machinery may be idealized as point sources in low frequencies, due to the fact that wave length of vibration is greater than length of engine mounts and isolators.

Caresta and Kessissoglu (2010) compared coupled finite element and boundary element method to analytical solution by using a submerged cylinder as a reference. Analytical and computational responses where found to be highly similar.

Blanchet and Caillet (2012) compared wavelet method and boundary element method for computational time and accuracy in coupled system. Wavelet method was found five times faster than boundary element method. Results obtained using wavelet approach differed slightly from result obtained using boundary element method. Authors concluded this is acceptable, when faster computational times are required.

Pirvosky et al. (2012) studied vibration of a ship hull. Results from finite element method model and measurements of two sister ships were compared. Generally simulation result were found to agree with the measurements on the ships. In some cabins, vibration levels were estimated to be higher. This error was probably caused by fittings on the cabin that were not included in the model. In two other cabins vibrations were higher than estimated. Source of extra vibration is assumed to be pressure fluctuation in pipes fixed on the roofs of the cabins. Frequency range studied was up to 50 Hz. In frequencies over 60 Hz, the computational cost was noted to be too expensive. Fluid interaction was added using semi-empirical method of added mass.

Çalışkan and Yayladere (2013) studied modal densities of simplified submarine hull in high frequencies. Modal densities were found to be high enough to warrant use of statistical energy analysis method in frequencies above 100 Hz.

Plunt introduced applicability of statistical energy analysis in the early design process (2014). There were three different pacing between longitudinal stingers in a hull of lightweight surface vessel. The problem was to reduce the thickness of hull plates to save weight. Spacing was found to have major influence in sound level, especially in low frequencies. Statistical energy analysis was found to be useful in providing noise level predictions in the early design phase, when the model is not established.

A hybrid method combining elements of both finite element method and statistical energy analysis was developed by Shorter and Langley (2005). Cotoni et al. (2007) studied applicability of this hybrid method combining elements of finite element analysis and statistical energy analysis in mid frequency range between 50 Hz and 300 Hz. Comparisons was made to average of Monte Carlo simulations and experimental data. Results obtained with the hybrid method were found to agree with pure finite element method model and the experimental measurements.

Various other methods are being developed for the mid frequency range. For example wave-based method developed by Desmet (1998) in his thesis and further developed by various authors, as introduced by Deckers et al. (2014). Developed methods are collected into a book edited by Desmet et al. (2012). Virtual statistical energy analysis method in the mid frequency range developed by Bies et al. was introduced by Borello (2014) Other statistical and deterministic methods are introduced by Pluymers (2006).

New methods being developed for high frequency range were discussed by Wachulec et al. (2000, p. 9). These included three methods based on envelope analysis and mean value method. The extension of original envelope analysis, complex envelope displacements analysis was studied introduced by Carcaterra and Sestieri (1997). Results obtained by studying a simple model with the envelope method were found to agree with experimental results (Carcaterra and Sestieri, 1997, p. 228).

Over time, there have been various studies of structure-borne sound in marine environment. The development of computational methods is visible in the studies. From tests on small scale, studies have been moved to comparisons against finite element method results or full scale models. Only in few studies comparisons were conducted against experimental data in real environment. Most of the reviewed work compared results to literature or other finite element methods. No studies were found where statistical energy analysis would have been used to predict underwater noise. No studies were found were both finite element method and statistical energy analysis would be used over a wide frequency range and compared to water loaded structure.

In the literature review, development on modeling of structure-borne sound was found to be active. New methods are being developed and established to industrial use. These promise reduction in calculation times and wider frequency ranges where one method is applicable. In low frequencies, finite element method is the established calculation method. Most interesting development is in the high frequency range; advances in this frequency region improve results in mid and low frequency ranges due development of hybrid methods. Methods used in this thesis, finite element method and statistical energy analysis, are well established.

3 Theoretical background of structure-borne noise

3.1 Introduction

The mechanics of sound are studied either by analyzing energies of vibration, or by studying wave behavior of the vibration. Energy analysis is an important tool for numerical modeling, as in energy analysis the state of the system is expressed with limited degrees of freedom. Studying wave behavior of the structure provides physical view of the problem. (Fahy and Gardonio, 2007, chap. 1)

The analytical solutions to the vibrational problems are derived from both methods, but they are limited to simple geometries. In this thesis, the analytical method is used to calculate modal response in low frequency range. Over time, available computational power has been increased, so the focus of calculations has been shifted to numerical methods, providing approximate solutions to the equations of motion. The numerical methods are divided by the theory used to obtain solution. Deterministic methods approximate solution to equations of motion. Statistical methods take random behavior of the vibration into account and usually analyze energies of the system by using principle of conservation of energy. (Fahy and Gardonio, 2007, chaps 1, 7.8, 8)

In this chapter theoretical foundation on the mechanics of noise and vibration is presented. Solution process and fundamental properties are discussed using both wave and energy theories. Octave bands, used to process measured or calculated data in frequency domain, and generation and transfer of noise in ships are discussed. Theory of the numerical methods used in this thesis and modeling of water loading is presented.

3.2 Sound as physical phenomena

Definition of sound by Fahy (2000, p. 6) is: “The phenomenon of *sound* in a fluid essentially involves time-dependent changes of density”. Instead of changes in density, the changes of density are measured as changes of pressure, temperature and position of particle. The derivatives of particle displacement lead to accelerations and velocities, used to measure response of a structure to excitation. Sound differs from other pressure changes, such as the changes of weather, by the rapid propagation through medium, called the *speed of sound,* also known as the *velocity of sound*. Sound is usually created when some structural vibration displaces fluid, creating local change in density. These disturbances propagate as waves, where disturbance from equilibrium is transferred without net transfer of mass. Sound is often transmitted via audio frequency waves in solids. This phenomenon is called *structure-borne sound*. The term includes also sound transmission in fluids, originating from structural vibrations. Modeling vibration in solids is more complicated than modeling vibration in fluids. (Fahy, 2000, chaps 2, 10.1)

3.3 Vibrating motion

Waves carry disturbance from equilibrium sensed as sound by transferring energy through a medium without transferring mass. The wave proceeds through the medium at a constant *phase velocity* c_p. Phase velocity is the function of displacement and time. The displacement is measured as *wave length* λ, the distance between wave crests presented in figure 6. Time t is measured as reciprocal of time called *frequency f,* $f = 1/t$, or *angular frequency* ω, $\omega = 2\pi/t$. *Amplitude* of vibration, X is the maximum disappearance from equilibrium. (Mansfield and O'Sullivan, 2011, pp. 278–279)

A compact way to define wave propagation in a medium is to use w*ave number k.* Wave number is the ratio of frequency ω and the phase velocity, c_p. Mathematical relation between time, wave length, wave number and frequency is presented in equation (1). (Mansfield and O'Sullivan, 2011, pp. 278–280)

$$c_p = \frac{\lambda}{t} = \lambda f = \frac{\omega \lambda}{2\pi} = \frac{\omega}{k} \tag{1}$$

Group velocity c_g is the velocity at witch the energy propagates. Group velocity is calculated using equation (2). (Fahy and Gardonio, 2007, p. 7).

$$c_g = \frac{\partial k}{\partial \omega} \tag{2}$$

In figure 6, the wavelength of sine wave is presented as a distance between two wave crests, at positions x_i and x_j on x axis of Cartesian coordinate system. (Mansfield and O'Sullivan, 2011, p. 278)

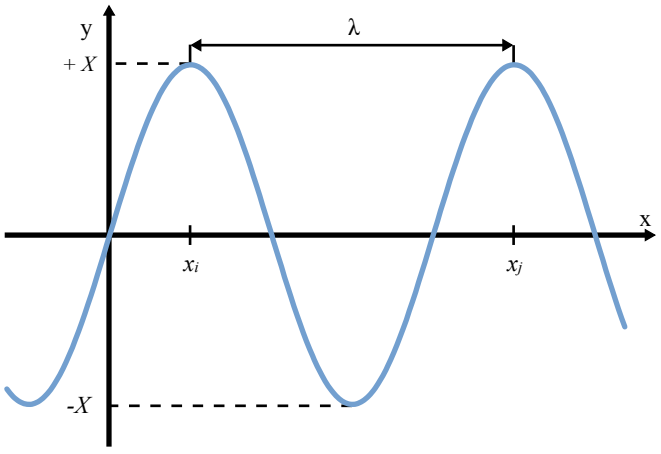

Figure 6: Amplitude X and wave length λ of sine wave in Cartesian x, y coordinate.

In engineering applications, the vibrational system is usually modeled as a set of springs, dampeners, and masses. Example of such system is a particle with mass M, bounded by spring constant K and dampening coefficient C. The system is excited by harmonic force F. Described system is presented in figure 7 and equation of motion for particle is presented in equation (3). Displacement of the system at any given time is solved from equation (3). (Biggs, 1994, chap. 2.1)

$$M\ddot{u}(t)+C\dot{u}(t)+Ku(t)-F=0$$
$$\ddot{u}(t)=\frac{d^2u}{dt^2} \quad \text{and} \quad \dot{u}(t)=\frac{du}{dt} \tag{3}$$

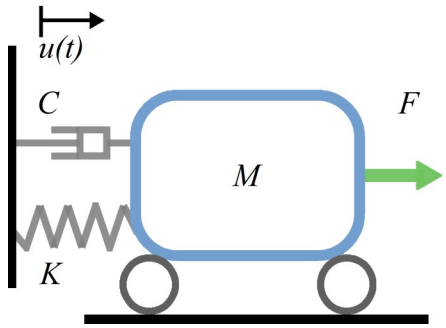

Figure 7: Forced response of dampened, vibrating system.

Equation (3) is extended to multidimensional systems and systems with more than one degree of freedom by using matrix equations. Equation (3) in matrix format is presented in equation (4). The extension to multidimensional problems is discussed by Biggs (Biggs, 1994, chap. 3).

$$\boldsymbol{M\ddot{u}+C\dot{u}+Ku-F}=0 \tag{4}$$

3.4 Modal analysis

To solve equation (3), modes of vibration are calculated from by setting damping coefficient C and force F to zero, reducing the differential equation to equation of free motion, presented in equation (5). Solution to differential equation presented in the equation (5), is presented in equation (41). Constants β_1 and β_2 are solved from initial conditions. (Biggs, 1994, chap. 2.2)

$$M\ddot{u}+Ku=0 \tag{5}$$

Solution to differential equation presented in the equation (5), is presented in equation (41). Constants β_1 and β_2 are solved from initial conditions. (Biggs, 1994, chap. 2.2)

$$u=\beta_1\sin(\omega_n t)+\beta_2\sin(\omega_n t) \tag{6}$$

Angular frequency ω_n at equation (41) is the *natural frequency* with order number n of the system. Natural frequency is a frequency where bounded, undamped system vibrates freely, in contrast to unbounded, undamped system that may vibrate freely at any frequency. Natural frequency is calculated from spring constant K and mass M. Natural frequency is the inverse of natural period, the time required for one complete cycle of free vibration. Natural frequencies have major effect on the forced response of the system, the greatest response occurs at natural frequencies. Equation for natural frequency is presented in equation (7). (Biggs, 1994, chap. 2.2; Fahy and Gardonio, 2007, chap. 1.10).

$$\omega_n = \frac{1}{2\pi}\sqrt{\frac{K}{M}} \tag{7}$$

Water loading has a great effect on modal properties of the structure. The Lewis formula, presented in chapter 3.9 of this thesis may be used to calculate the effect of water loading for analytical solution. Most of the structures may be modeled assuming structures either plate- or beam-like. For a beam, the natural frequencies may be calculated using Euler-Bernoulli relation. The relation omits the effect of shear stress. The natural frequencies are calculated using elastic modulus of the beam E, area moment I, and distributed mass m. Equation for a beam supported by hinges is presented in equation (8) where n is any integer between one and infinity describing the number of studied natural frequency. (Biggs, 1994, p. 154)

$$\omega_n = \left(\frac{n\pi}{L}\right)^2\sqrt{\frac{EI}{m}} \tag{8}$$

Natural frequencies for circular plate are calculated from Kirchhoff relation. The relation omits the effect of shear stress. Natural frequencies are calculated using plate stiffness D_e and thickness h. Equation for bending stiffness for a plate is presented in equation (9). (Soedel, 2004, pp. 27, 129)

$$D_e = \frac{Eh^3}{12(1-\nu^2)} \tag{9}$$

Equation to calculate natural frequencies for circular plate with radius r is presented in equation (10). Eigenvalues λ are calculated from boundary conditions. (Soedel, 2004, p. 129).

$$\omega_n = \left(\frac{\lambda}{r}\right)^2\sqrt{\frac{D_e}{mh}} \tag{10}$$

Mode count $N(\omega)$ is expected number of modes, or natural frequencies, below frequency, ω. *Modal density*, $n(\omega)$ is expected number of modes, or natural frequencies in a bandwidth $d\omega$. Modal density describes the energy storage capability of a subsystem. Relationship between mode count and modal density is presented in equation (11). (Lyon and DeJong, 1994, p. 11)

$$n(\omega)=\frac{dN(\omega)}{d\omega} \tag{11}$$

Modal analysis for multidimensional systems and systems with more than one degree of freedom is preformed by using matrix equations as is discussed by Biggs (1994, chap. 3.7).

3.5 Forced vibration

All physical systems are limited by boundaries, and many systems have the changes of material properties, or the geometry inside of the system. Wave can not travel through these non-uniformities or boundaries unchanged. These interactions create refraction, diffraction, reflection, and scattering. Structurally, the most important is reflection, as waves reflecting on boundaries create *resonance*. The resonance of a system occurs at any input frequency corresponding to natural frequency of the system in free vibration. If the system is not damped, the response caused by input at natural frequency is unlimited. The greatest response levels occur at natural frequencies, creating fatigue problems and affecting human comfort. (Fahy and Gardonio, 2007, chaps 1.10, 1.11; Bertram, 2011, chap. 5.4)

For a dampened system excited with constant impulse *F*, the solution to equation (3) is obtained by assuming dampened natural frequency and un-dampened natural frequency approximately equal, $\omega_d \approx \omega_n$. The solution is written using critical dampening, ξ and is presented in equation (12). (Biggs, 1994, p. 55)

$$u=\frac{F}{k}\left[1-e^{-\xi t}\left(\cos(\omega_n t)+\frac{\xi}{\omega_n}\sin(\omega_n t)\right)\right] \tag{12}$$

Solution using pulsating force is introduced by Biggs (1994, chap. 2.5).

3.6 Transfer of vibration

Vibration proceeded in three dimensional solids in two wave types, longitudinal and shear waves. In geometries, where one dimension is larger compared to other dimensions, such as beams, and in geometries, where two dimensions are larger, namely plates, third type of vibration is created. Boundary conditions due to dimensions of the geometry creates bending waves. Of these three wave types, bending wave is the dominating wave type in transfer of vibrational energy from machinery to hull in low frequencies. Main assumptions in Timoshenko beam and Mindlin plate is that cross-sectional planes stay planes, but not 90° degrees to center-line. Progression of bending wave in Timoshenko beam or Mindlin plate is presented on figure 8. (Ross, 1987, chap. 5.1)

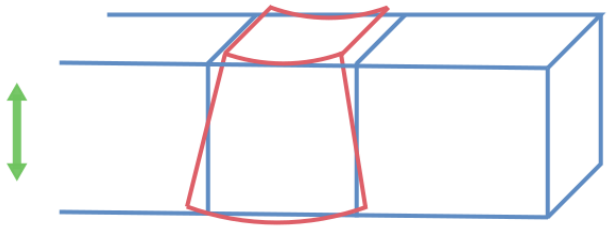

Figure 8: Bending wave on thin Timoshenko beam or thin Mindlin plate. Wave progresses from left to right, arrow indicates main direction of vibration. (Modified from Linjama, 1991).

Every wave type has characteristic phase velocity, describing the velocity vibration travels in solid. Phase velocity of bending waves in a beam is derived from bending equation for Timoshenko beam. In Timoshenko beam theory, the beam is assumed to be uniform or nonuniform with negligible spatial derivatives of moments of inertia. In low frequencies, shear parameters and relative rotatory terms are assumed to be small, leading to Euler-Bernoulli beam equation. From Euler-Bernoulli beam equation the phase velocity of bending vibration is solved. The solution for phase velocity in a beam is presented in equation (13). The solution assumes the shear stiffness does not have any effect on results. (Ross, 1987, chaps 5.3–5.4)

$$c_{p,beam} = \sqrt[4]{\frac{\omega^2 EI}{m}} \tag{13}$$

Mindlin plate equation assumes constant thickness in bending and plane stress conditions. The equation is solved to provide phase velocity of bending vibration in a plate in low frequencies. The equation for phase velocity in a plate is presented in equation 14. Equation (13) is the Kirchhoff equation for plate, the equation assumes shear stiffness has no effect. (Ross, 1987, chap. 6.1; Fahy and Gardonio, 2007, chap. 1.7)

$$c_{p,plate} = \sqrt[4]{\frac{\omega^2 D_e}{m}} \tag{14}$$

From equations (13) and (14), the factors effecting the most dominant vibration mode, bending vibration, are visible. In addition to distributed mass and frequency, the material ability to resist stresses affects the transfer of vibration in ship structures.

3.7 Statistical energy analysis

3.7.1 Energy equations

To calculate response of random vibrations in diffused reverberant field, statistical energy analysis (SEA) has been developed. SEA approximates time-averaged response of the system using analysis of power balance between subsystems. Subsystems consists of different material properties and geometries. Subsystems coupled together create a larger system. SEA yields the best results in cases where the system has high modal

density. Coupling between the subsystems is most readily calculated when coupling between subsystems is weak, but solutions also exists strongly coupled systems. (Fahy and Gardonio, 2007, chap. 7.8)

Energy flow between subsystems is written as averaged power balance using principle of conservation of energy. The power balance for system j is written using power input $P_{\text{in},j}$, the transferred energy to other subsystems $\sum_k P_{jk}$, and power dissipated in the subsystem $P_{diss,j}$. The power balance is presented in equation (15). (Lyon and DeJong, 1994, p. 64).

$$P_{\text{in},j} = P_{diss,j} + \sum_k P_{jk} \tag{15}$$

Power dissipated in the subsystem j is described using *damping loss factor* η_j, measuring the rate of energy dissipation in the system j, and energy stored in the subsystem, E_j. In equation (16) power flow P_{jk} between subsystems j and k is written using *coupling loss factor* η_{jk} of energy transfer between systems j and k. Coupling loss factors are usually calculated from wave transmission coefficients. Variable n_j is the modal density of system j, indicating the number of natural frequencies in a frequency band. Modal density is defined on equation (11). The power balance of equation (15), written using the definitions of power flow and transferred energy is presented in equation (16). (Lyon and DeJong, 1994, pp. 64, 120)

$$P_{\text{in},j} = \omega \eta_j E_j + \sum_k \omega \eta_{jk} n_j \left(\frac{E_j}{n_j} - \frac{E_k}{n_k} \right) \tag{16}$$

Modal densities and coupling loss factors reciprocate. This principle of reciprocate of SEA is presented in equation (17) (Lyon and DeJong, 1994, p. 64).

$$n_1 \eta_{12} = n_2 \eta_{21} \tag{17}$$

The power balance between the two subsystems with average energies E_1 and E_2 is written by extending equation (15). The extension is presented in equation 18 using the matrix form and is illustrated in figure 9. (Lyon and DeJong, 1994, p. 64)

$$\begin{bmatrix} P_{\text{in}1} \\ P_{\text{in}2} \end{bmatrix} = \begin{bmatrix} P_{diss,1} + P_{12} \\ P_{diss,2} + P_{21} \end{bmatrix} = \begin{bmatrix} \omega \eta_{12} E_1 + P_{12} \\ \omega \eta_{21} E_2 + P_{21} \end{bmatrix} \tag{18}$$

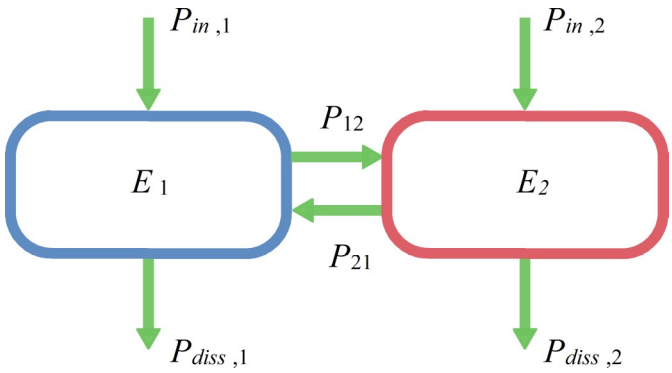

Figure 9: Power balance between two subsystems.

The power balance equation for multiple subsystems is a matrix equation. After damping and coupling loss factors, subsystem masses and modal densities the SEA are determined, the matrix equation is readily solved. From the vibrational energies of subsystems, dynamical results, such as averaged magnitude of response are calculated.

3.7.2 Modal densities

Modal densities are dependent on the geometry of the system and the boundary conditions. For one dimensional (1*D*) system the geometry parameter is *L*, for two dimensional (2*D)* system the geometry parameter is area *A*. Equations used to calculate modal densities for one and two dimensional subsystems are presented in equation (19). (Lyon and DeJong, 1994, pp. 137, 139–140)

$$n(\omega)_{1D} = \frac{L}{\pi c_g}$$
$$n(\omega)_{2D} = \frac{A\omega}{2\pi c c_g} \qquad (19)$$

3.7.3 Coupling loss factors

Coupling loss factor is used to calculate the transmission of wave between different subsystems of a SEA system and point excitations connected to the system. At the edge, the wave will partially reflect and partially transmit to outgoing waves in the connected elements. This behavior is represented by t*ransmission coefficients. C*oupling loss factor is calculated from transmission coefficient, assuming the vibration field is fully diffused. In a typical SEA system structural subsystems are connected via point, line and area connections. (Langley and Heron, 1990)

Point connections, marked in red, and line connection, marked in green, between subsystems E_1 and E_2 are illustrated in figure 10 a). Area connection, marked in green, between subsystems E_1 and E_2 is illustrated in figure 10 b).

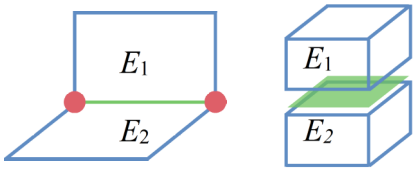

Figure 10: Two panels, subsystems E_1 and E_2, connected by point connections, presented in red, and line connection, presented in green, illustrated in figure a). Structural subsystem E_1 and acoustic subsystem E_2, connected by area connection, presented in green, illustrated in figure b).

Transmission coefficient for line and point junctions is calculated from the amplitude of vibration, *X*. Amplitude is solved from equations of motion and compatibility conditions. A dynamic stiffness matrix is used to connect forces and displacements at the edges of elements. Transmission coefficient is of a form presented in equation (20), where *i* and *j* represent plates. Wave type is represented by *p*, angular frequency by ω and heading of the indecent wave by ϕ . Wave type of generated wave is represented by *r*. (Langley and Heron, 1990; Langley and Shorter, 2003)

$$\tau_{pr}^{ij}(\omega,\phi) \tag{20}$$

Line junctions connect edges of beam–plate and plate–plate junctions. Plates may be connected directly or via a beam at the connection. The equations of motion are solved using Fourier transform to provide transmission coefficients for line junctions. The equations of motion include effects of shear deformation, rotary inertia, and wrapping. Offset between plate attachment line and shear axis is taken into account. Coupling loss factor η_{pr}^{ij} for isotropic infinite beams and semi-infinite plates is calculated from transmission coefficient using equations (20) and (22). (Langley and Heron, 1990)

$$\eta_{pr}^{ij} = \frac{c_g L \tau_{pr}^{ij}(\omega)}{\pi \omega A_i} \tag{21}$$

$$\tau_{pr}^{ij}(\omega) = \frac{1}{2}\int_0^{\pi} \tau_{pr}^{ij}(\omega,\phi)\sin(\phi)\,d\phi \tag{22}$$

Curved shells are not semi-infinite, thus for curved shell, the semi-infinity condition is fulfilled by assuming that the wave field is completely absorbed by the opposite edge from the connected edge. Love-Timoshenko shell theory is used to provide equations of motion for non-isotropic curved shell. For a junction with length *L*, the coupling loss factor is calculated using equation (23). (Langley, 1994)

$$\eta_{ij} = \left(\frac{L}{4\pi^2 n_i}\right)\int_{\theta_i}\left[\frac{\tau_{ij}(\theta_i)c_{gy,i}(\theta_i)}{c_i(\theta_i)c_{g\theta,i}(\theta_i)}\right]d\theta_i \tag{23}$$

$$c_{gx} = c_g\cos(\theta_e), \quad c_{gy} = c_g\sin(\theta_e) \quad c_{g\theta} = c_g\cos(\theta-\theta_e)$$

A method to take into account in evenly spaced finite line connections is discussed by Heron (1997).

When a point junction has more than one degree of freedom, transmission coefficient is calculated using a wave based method. The analysis assumes structural subsystems are connected to the junction via number of massless, rigid disks. Every disk has six degrees of freedom, movements to all three directions of axes of Cartesian coordinate and rotation around all three axes of the Cartesian coordinate system. In an extension to a one dimensional (1*D*) wave represented in Cartesian coordinate system, a two dimensional (2*D*) wave is described in cylindrical coordinates. These type of waves may appear in plates. (Langley and Shorter, 2002, 2003)

Coupling loss factors for point connections depend on the dimensions of the connected subsystems. The conversion from transmission coefficient is calculate using the area of two dimensional junctions A, the length of the one dimensional junction L, angular frequency ω, phase velocity c_p and group velocity c_g. The equations used to calculate coupling loss factors are presented in equation (24). (Langley and Shorter, 2003)

$$\begin{aligned}
\eta_{jk} &= \frac{c_{g,j} c_{p,j}}{\omega^2 A} \left(\sum_{r_j} \tau_{kr,j} \right); \quad 2D_j \rightarrow 1D_k \\
\eta_{kj} &= \frac{c_{g,k}}{2\omega L} \left(\sum_{r_j} \tau_{kr,j} \right); \quad 1D_k \rightarrow 2D_j \\
\eta_{jk} &= \frac{c_{g,j} c_{p,j}}{\omega^2 A} \left(\sum_{r_j} \tau_{kr,j} \right); \quad 2D_j \rightarrow 2D_k
\end{aligned} \tag{24}$$

Structural-acoustic systems are connected through area connections. Coupling loss factor for area connection is calculated using equation (25). Density ρ_0 and wave velocity c_0 are properties of the fluid *0*. Distributed mass m is the property of structural element, plate. Radiation efficiency σ_{rad} is calculated from the time-averaged integral equation of power flow from surface to compressive fluid. (Leppington, Broadbent and Heron, 1982, p. 249; Henry, 2015)

$$\eta_{12} = \frac{\rho_0 c_0}{\omega m} \sigma_{rad} \tag{25}$$

When acoustic wave number k_a *i*s larger than plate wave number $k_p = \sqrt{k_x + k_y}$ the system is above coincident. When acoustic wave number is lower than wave plate number, the system is below coincident. Instead of k_x and k_y dimensionless wave numbers α_k and β_k are used, and this conversion is presented in equation (26). (Leppington, Broadbent and Heron, 1982, p. 250)

$$\alpha_k = \frac{k_x}{k_p}, \quad \beta_k = \frac{k_y}{k} \tag{26}$$

Connection l_k between dimensionless wave numbers α_k and β_k in polar coordinates (r, θ) is presented in equation (27). (Leppington, Broadbent and Heron, 1982, pp. 250–251)

$$l(\theta)_k = 1 - \alpha_k \cos\theta - \beta_k \sin\theta \tag{27}$$

When the system is above coincidence, acoustic wave number is assumed to approach infinity, $k_a \rightarrow \infty$, the area integrals of power-flow equation are approximated by $(2\pi l)^{-1}$. This results an approximation of radiation efficiency above coincidence, presented in equation (28). (Leppington, Broadbent and Heron, 1982, pp. 254–255)

$$\sigma_{rad} \sim \sqrt{1 - \alpha_k^2 - \beta_k^2} \tag{28}$$

Below coincidence, the radiation efficiency is calculated using factors A_k and B_k, relating plate geometry and wave number. Acoustic wave number is assumed to approach infinity. The formulas for radiation efficiency below coincidence are presented in equation (29).

$$\begin{aligned} \sigma_{rad} &\sim 2B_k, \quad k \rightarrow \infty, \alpha - k > 1, \beta_k < 1 \\ \sigma_{rad} &\sim 2A_k, \quad k \rightarrow \infty, \alpha_k < 1, \beta_k > 1 \\ \sigma_{rad} &\sim 2(A_k + B_k), \quad k \rightarrow \infty, \alpha_k < 1, \beta_k < 1 \end{aligned} \tag{29}$$

Equations (28) and (29) are not valid near coincidence, where $k_a = k_p$ (Leppington, Broadbent and Heron, 1982, p. 268). The solution near coincidence is discussed by Leppington, Broadbent and Heron (1982, p. 265).

3.8 Finite element method

Finite element method approximates equilibrium equation in a weak form. In weak form the solution is not calculated on every point of continuum, instead the solution is calculated on set number of discrete points, called *nodes*. This approximation is valid on small displacements. Element space between nodes is dived to number of elements, called *mesh*. On special occasions the nodes may be also located on lines defining the elements. Example of simply supported beam divided to 4 rectangular elements is presented in figure 11. The 10 connecting nods are marked in red. (Zienkiewicz *et al.*, 2013, chap. 3)

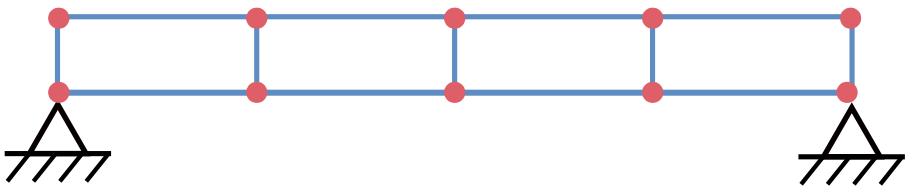

Figure 11: Simply supported beam divided to 4 rectangular elements. The 10 nodes connecting the elements are presented in red.

Monte Carlo simulation may be used to capture random behavior of the structure under vibration. In the simulation the problem is solved multiple times and the average of the solutions is the most probable one (Fishman, 2008).

Finite element method approximates the matrix equation of motion in multidimensional problem, presented in equation (4). The equation is written in terms of mass matrix ***M***, stiffness matrix ***K***, damping matrix ***C*** and load matrix ***F***. The matrices are derived from functionals Π, specific to type of element used. For fluids equation (4) is written as the function of global acoustic inertia ***Q***, global damping ***D*** and global stiffness ***H***. Volumetric excitations generated in the fluid are represented by ***q***. FEM is valid only on closed acoustic volumes. Structural and acoustic finite element equations are connected via coupling matrices ***S*** and ***R***. (Cook, Malkus and Plesha, 1989, chaps 18.6, 18.9; Zienkiewicz *et al.*, 2013, chaps 3, 12)

Functionals are calculated from the weak form of equilibrium equation in one dimensional elements, such as a beam is a simplification of three dimensional equilibrium equations in Cartesian coordinates. The equation is written using density ρ and elastic modulus E. The structure is loaded with a body force b_x. In addition to assuming one dimensional expression, the weak form of equilibrium equation neglects the transverse shear deformation. The functional equation for one dimensional problem is presented at equation (30). An arbitrary function $w(x)$ is introduced in the equation (30). The function is defined on the domain of the equilibrium equation Ω. Function $w_b(x)$ for node b is zero on every other node of the system (Zienkiewicz *et al.*, 2013, chaps 2.2.4, 3.2.1)

$$\Pi = \int_{\Omega} w(x)\left(\rho \frac{\partial^2 u}{\partial t^2} - b_x\right) dx + \int_{\Omega} \frac{\partial w}{\partial x} E \frac{\partial u}{\partial x} dx = 0 \tag{30}$$

Equilibrium equations for plate are simplified by assuming that plane sections normal to the middle plane remain plane during the deformation. The rotary inertia is omitted because plate thickness h is assumed to be thin compared to other dimensions. Equation of weak form with zero forces is presented in equation (31). (Zienkiewicz *et al.*, 2013, chaps 13.2.1, 13.3.2)

$$\Pi = \int_{\Omega} \delta w \rho h \ddot{w} d\Omega = 0 \tag{31}$$

Weak form of acoustic equation approximates Helmholtz equation for pressure of fluid p. In the weak form equation wave amplitude is assumed to be small and effects of viscosity are omitted. The functional equation is presented in equation (32). (Cook, Malkus and Plesha, 1989, chap. 18.6)

$$\Pi = \int_{V} \delta w (\nabla^2 p + k^2 p) = 0 \tag{32}$$

Finite element approximation of equations (30) and (31) are discussed by Zienkiewicz et al. (2013, chap. 3.4, 13.3.3). Finite element approximation of equation (32) is discussed by Cook et al. (1989, chap. 16.8). The solution process of dynamic finite element approximation of equation (4) is discussed by Zienkiewicz et al. (Zienkiewicz *et al.*, 2013, chap. 12).

3.9 Fluid loading of vibrating structure

Relatively dense fluid around a structure can alter the vibrational properties of the structure significantly, especially at lower frequencies. Mass of entrained fluid increases the mass of the structure. natural frequencies and impedance change as the mass increases. If water depth is shallow, approximately less than five times the draft of the ship, the effect of water floor increases the added mass. If the volume of the surrounding fluid is large, finite element method is not feasible due to computational time. (Fahy and Gardonio, 2007, chap. 3.13; Lloyd's Register, 2015, chaps 4.4, 4.5)

The fluid loading of the structure is solved either by calculating pressure radiating to the fluid by the structure, or by calculating added mass. For baffled pistons and plates the radiated pressure is solved from Rayleigh integral, presented in equation (33) (Fahy and Gardonio, 2007, p. 141; Langley, 2007, p. 766).

$$p(\boldsymbol{x}) = -\left(\frac{\rho\,\omega^2}{2\pi}\right)\int_A \left(\frac{e^{-jkr}}{r}\right) w(\boldsymbol{x}')\,d\boldsymbol{x}', \quad r = |\boldsymbol{x} - \boldsymbol{x}'| \tag{33}$$

Equation (33) connects pressure at any location $\boldsymbol{x}$ of space to out of plane displacement $w(\boldsymbol{x})$ at any location $\boldsymbol{x}'$ on the surface of structure. (Fahy and Gardonio, 2007, p. 141; Langley, 2007, p. 766)

If the structure is more complex, fluid loading may be calculated using added mass. The equation for added mass written using deflection $\boldsymbol{u}$ and the amplitude of osculating vibration X. Vector $\boldsymbol{n}$ is normal pointing from the fluid to hull. The fundamental equation for added mass is presented in equation (34). (Ross, 1987, chap. 5.10; Bertram, 2011, chap. 5.5)

$$M_A = \sum \int_S \frac{1}{\omega^2} X\,\boldsymbol{n}\boldsymbol{u}\,dS \tag{34}$$

Solution to equation (34) is approximated using Lewis' formula, where the added mass is written using water density ρ and shape parameters a, b and t describing size and shape of the hull. Lewis' formula is presented in equation (35). (Bertram, 2011, p. 227)

$$M_A \sim \rho\frac{\pi}{2} r^2\left[(1-a^2)+3b^2\right] \tag{35}$$

Shape parameters a, b and r are solved from system of non-linear equations relating to cross-section width in the waterline B, draft $T(y=0)$ cross-section coefficient C_M. The system of non-linear equations is presented in equation (36). (Bertram, 2011, p. 227)

$$\begin{cases} \dfrac{B}{2T} = \dfrac{1-a+b}{1+a+b} \\ C_m = \dfrac{\pi}{4}\dfrac{1-a^2-3b^2}{(1+b)^2-a^2} \\ r = \dfrac{B}{2(1-a+b)} \end{cases} \tag{36}$$

Cross section coefficient is ratio of cross-section area A_{cc}, cross-section width B and draft $T(y=0)$. The ratio is presented in equation (37). (Bertram, 2011, p. 227)

$$C_M = \frac{A_{cc}}{BT} \tag{37}$$

Radiating pressure from irregular shaped structures is calculated using Kirchhoff-Helmholtz integral equation. The integral equation is presented by Fahy and Gardonio (2007, chap. 3.13). Analytical solution to the Kirchhoff-Helmholtz equation is available only for simple geometries. For complex structures the solution is approximated using boundary element method. (Fahy and Gardonio, 2007, chaps 3.13., 8,7)

Boundary element method is computationally heavy but it provides a tool to model forces interacting from fluid to structural elements. These forces may be caused from hydrodynamic loads or reflections of pressure from bottom of water. For faster solution times, wavelet method is is used. Wavelet method approximates solution to Rayleigh equation, presented in equation (33), the approximation reduces accuracy when compared to boundary element method. Also, the wavelet method may be used to model only vibrations of hull plates, but not the radiation of noise from ship to water. (Blanchet and Caillet, 2012)

Force is calculated from Rayleigh equation (33) using displacement u_m and area A. The radiated pressure is derived for a generalized force acting on the degree of freedom a_m due surface pressure created by motion of a system. If the surface is an infinite plane with zero displacement outside the plate the force describing water loading is presented in equation (38). (Langley, 2007, p. 767)

$$f_m = \int_A p(\boldsymbol{x}) u_m(\boldsymbol{x})\, d\boldsymbol{x} = \sum_n D_{mn} a_n \tag{38}$$

Assuming radially symmetric shape function, the stiffness matrix D_{mn} in equation (38) is presented in equation (39) using Greens' function $G(k)$. (Langley, 2007, p. 768).

$$D_{mn} = \frac{1}{2\pi} \int_0^\infty G(k) |U(k)|^2 J_0(k r_{mn})\, k\, dk, \quad r_{mn} = |\boldsymbol{x_m} - \boldsymbol{x_n}| \tag{39}$$

3.10 Generation of noise in ships

Ship has a number of noise and vibrational sources; the main sources affecting ship hull vibrations are sea-way, prime mover, and propeller. Other special conditions where vibrations are generated include flow separation at the structural joints and torque fluctuations in electric engines. Airborne noise is mainly generated in operation of machinery, but also in operation of air conditioning, exhausts, and intakes. (Carlton and Vlašić, 2005; Bertram, 2011, chap. 5.6)

In high travel speeds, propeller noise dominates the noise profile of the ship. As the travel speed increases, the pressure around the propeller decreases. When pressure is sufficiently low, cavities begin to form and fill with the air around the propeller. This creates rapid succession of explosions and implosions, creating noise and vibrations. In addition to propellers, cavitation occurs in locations along ship hull where locally high

velocities appear, including rudders, shaft brackets, and hydrofoils. (Ross, 1987, chap. 8.6; Bertram, 2011, chaps 2.4, 5.6)

Main mechanical vibrational sources are in the power line. These include engines and generators, gear boxes, propeller shaft, propeller, and auxiliary equipment. Diesel engines are divided to low and high speed engines. Slow speed engines are used in large cargo ships, because they provide more power and better economics. Slow speed engines are large at size and heavy, fastened directly to the ship hull. Medium and high speed diesel engines do not have structural imbalances causing global vibrations and may be installed on dampening mounts. Thus, they are used in passenger, naval, and research vessels, where low vibrational levels are required. Medium and high speed engines are connected to the propeller via gear box, adding another vibrational source. Electrical and turbine engines do not contribute significantly to the vibration of ship. Main mechanical vibrational creation mechanisms include mechanical unbalances, electromagnetic and pressure fluctuations, impacts, and friction. The most dominant mechanisms are impact of piston against cylinder, known as piston slap, and mechanical imbalances. (Fischer and Collier, 2007; Lloyd's Register, 2015)

3.11 Transfer of noise in main structural elements of ships

Vibrations of ship hull are divided to global and local vibrations. Global vibrations involve whole structure. For a structure symmetric along center-plane, such as the reference structure used in this work or a typical ship, three main types of global vibration are identified: vertical, horizontal, and torque. Local vibrations involve elements of the structure, such as bulkheads. (Bertram, 2011, pp. 5.3, 5.4)

Noise and vibrational transfer paths are categorized to airborne, structure-borne and waterborne transfer paths. Underwater- and airborne noise is created from vibrations of ship hull. Direct path transfers vibration of machinery via foundation to parts of ship structure in contact with the fluids surrounding the ship. Vibrations of machinery set surrounding air into vibrating motion creating airborne noise. Vibrations of air excite the structure, leading to further underwater and airborne noise, creating second structural transfer path. Different excitation paths from a machinery are illustrated in figure 12. (Fischer and Collier, 2007)

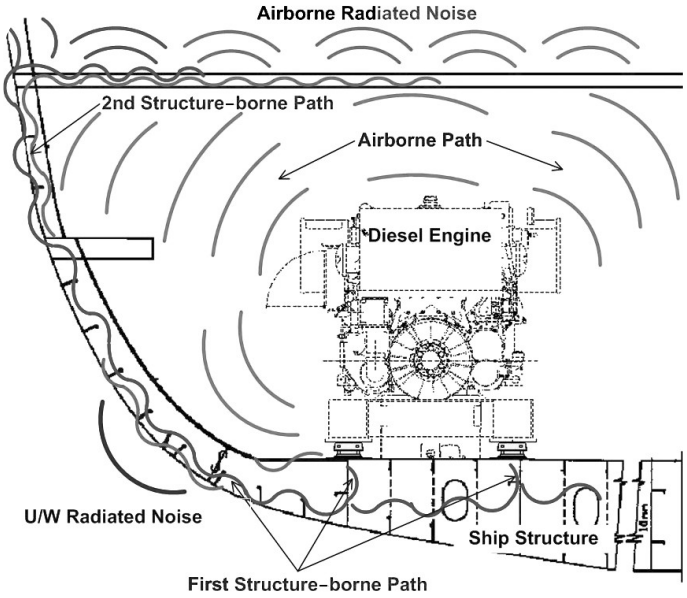

Figure 12: Noise and vibrational transfer paths from ship engine. (Fischer and Collier, 2007, p. 1217)

3.12 One third octave bands and decibels

Measurements or calculations may be presented using logarithmic units if scales of obtained values are very large. Decibels relate obtained value to a reference value. The relation used to convert ψ to decibel value ψ' is presented in equation (40). (Ross, 1987, chap. 1.2)

$$\psi' = 10 \log_{10} \frac{\psi}{\psi_{ref}} \tag{40}$$

In water pressure reference value presented in equation (10) is used. (Ross, 1987, chap. 1.2)

$$p_{ref} = 10^{-6} \text{ Pa} \tag{41}$$

In frequency analysis, frequency domain is represented octave bans or one third octave bands. If more information is required, narrower one third octave bands are used. Lower frequency limit f_l and upper frequency limit f_u of one third octave bands are calculated using ratio presented in equation (42). (Bies and Hansen, 2003, p. 43)

$$\frac{f_u}{f_l} = \sqrt[3]{2} \tag{42}$$

The bandwidth *df* of one third octave bans is calculated using equation (43) and center frequencies f_c from table 1. (Bies and Hansen, 2003, p. 43)

$$df = f_c \frac{\sqrt[3]{2}}{\sqrt[6]{2}} \tag{43}$$

To avoid bins with factories, values calculated using equation (40) are adjusted to preferred values. Preferred center frequencies and upper and lower limits on one third octave band are presented in table 1.

Centre Frequency (Hz)	Lower Band Limit (Hz)	Upper Band Limit (Hz)
16	14.25	17.96
20	17.82	22.45
25	22	28
31.5	28	35
40	35	44
50	44	57
63	57	71
80	71	88
100	88	113
125	113	141
160	141	176
200	176	225
250	225	283
315	283	353
400	353	440
500	440	565
630	565	707
800	707	880
1000	880	1130

Table 1: Preferred one third octave frequency bands. (Bies and Hansen, 2003, p. 43)

4 Creating model for predicting structure-borne sound

4.1 Introduction

The development of VA One was started in 2001, with the first release in 2003. VA One begun from development on older technologies, AutoSEA2 and Rayon Solver. In VA One, lower and higher frequency analysis methods are combined to provide hybrid methods to mid frequency range. VA One provides links to external software in all steps of modeling process. (ESI Group, 2003, 2013, 2015; Henry, 2015)

Statistical energy analysis in VA One solves energy balance equation (16) using VA One SEA solver. Calculation method used to calculate modal densities is presented in equation (19). Method used to determinate the coupling loss factors is discussed in chapter 3.7.3 of this work. COSMIC NASTRAN (1981) solver is used to solve the finite element form of equilibrium equation. The solution is calculated in two parts: first modal solution, described in chapter 3.4 of this work, is calculated. After modal solution is found, forced response, described in chapter 3.5, is solved. Water loading is calculated using wavelet method, presented in equations (38) and (39) of this work.

4.2 Structural elements

In VA One, structural elements are imported as computer aided design geometry or finite element geometry. The model may be also created directly in VA One using nodes and build-in scripts. Finite element model is created either by using external program or from SEA model using VA One.

Shell elements are available at VA One in three different geometric forms, plates, cylinders and curved shells. Beam elements are available directly or by using reinforced plates. Surface regions in finite element are modeled using FE faces. Surface region may represent connection of structure to fluids or represent region where noise control treatment is added. If possible, element length of FE face near the structure should be the same as element length on the subsystem FE face is connected to.

4.3 Fluid elements

Fluids are modeled using FE and SEA acoustic cavities for small closed volumes. Water loading of the structure is modeled using semi infinite fluid (SIF) element. SIF element is a wavelet based energy absorbing sink, proving dampening for SEA elements and dampening and water loading for FE elements. For SEA model only SIF element is needed to model water-structure interaction. The dynamic behavior of fluid can be fully described using speed of sound and density. For numerical analysis of fluid mechanical problems, various thermal and chemical properties of the fluids are required.

4.4 Special features of statistical energy analysis model

SEA model may be created from imported finite element or CAD geometry. SEA models may be also created directly in VA One. Acoustic SEA cavities that may be created are inside spaces defined by structural elements.

SEA elements representing energy storing subsystems are connected through coupling loss factors, transferring energy between subsystems. Line and point junctions connect panels and beams together. Area junction connects acoustic elements to other acoustic elements or to structural elements. VA One calculates coupling loss factors automatically using equations presented in chapter 3.7.3 of this work. Infinite or semi-infinite assumption of line and point connections is assumed to be met when structural elements are connected on all sides, thus there are no free edges in the model.

4.5 Special features of finite element model

Fluid elements are connected to structural elements using FE faces defining surface of region. In addition, FE junctions are used to connect structural elements and acoustic elements. FE junctions represent coupling matrices connecting acoustic and structural FE equations.

Generating mesh is a fundamental step in FE-modeling. It affects directly the quality of the results and has a great impact on time used to solve the problem. FE-mesh of vibrational problem should be homogenous as any heterogeneity, such as small strips in the field of larger square elements, has potential to break the transfer path of the vibration. Square elements has been found to provide best results in structural models, but parallelograms will also work, when angles do not greatly differ from right angles. The best results for fluids are obtained by using triangular elements. Aspect ratio between structural and fluid elements should be small, preferably 1.

Coarse mesh, including only the main structural parts, is used in global structural analysis in higher frequencies. Fine mesh, with small details, is used to capture effects of higher frequency vibration in small elements of the structure. In the model of structure-borne sound, mesh density is expressed as element length. The length is calculated as fractions of wave length λ defined in equation (42). Thus, element length depends on maxim frequency of the simulation and the phase velocity of the vibration in the medium. In practice, the speed of sound in the medium is used to estimate phase velocity. Wave length is divided with mesh density factor n to provide a desired element length. Optimal range for n, the *mesh density factor*, is between 4 and 10, with the best initial value at 6. Maximum limit of element length is presented in equation (44).

$$d_{element} < \frac{\lambda}{n}, \quad n \in [4, 10] \tag{44}$$

Defining material property in mesh density is the phase velocity of the medium. In marine applications, modeling water loading is usually necessary, leading to coupled problem. In hull, the speed of sound is high and mesh could be relatively coarse. In water, the velocity of sound is lower and thus finer mesh is needed to reach solution in same frequency range, when hull is loaded with water. This property can be used to optimize the mesh by dividing the model on waterline. Structure above waterline could be modeled using relatively low mesh density while structure below waterline is modeled using a high mesh density.

4.6 Loads and sensors

Loads are inserted to the nodes of FE structures and FE acoustic cavities or FE element or SEA elements. Load sources available in VA One include distributed loads caused by fluid dynamics and point forces, used in this work. Point forces and moments transfer energy via point connection to structural vibration. They are used to model dynamic forces and moments acting on surface of structure and have value as function or constant. Point forces are also used to model distributed mass from ship equipment and machinery. Also various aero- and hydrodynamic pressure disturbances, created in liquid, air or in the fans and ducts, are available. Load functions may be created externally or may be imported from other software or measurements.

Response of the finite element model is recorded using sensors and FE faces. Sensors are added to nodes and elements of FE structures. Sensors act as virtual strain gauges, microphones, or others sensors.

4.7 Results from the model

The solution is calculated in selected frequency domain, in center frequencies of selected octave band. Results calculated in a narrow band may interpolated to wider band later, if needed.

Finite element solution is calculated in two parts. First, forces and excitations are set to zero and water loading is activated to solve modal response of the system. Modal response calculates natural frequencies and modes of the vibration. Modal shapes obtained in modal analysis and all loads are used as initial data in the next solution step, forced response. Modal solution may be calculated using VA One or imported from other solver. SEA solution for modes and vibrations is available in one step.

Results from FEM analysis are natural frequencies and natural modes presented as lists. Modes are also animated. The vibrational response is recorded by sensors located at the nodes close to those of location of accelerometers in the sea trials. Vibrational response is provided as an average over selected element. Also various modal results and pressure levels at location of wavelet element are available.

5 Model of reference structure

5.1 Reference structure

The reference structure is a cylinder that can be submerged to required water level using ballast tanks and can be instrumented with accelerometers and noise and vibration sources. On the top of the cylinder is an access hatch to instrument space. The reference structure is presented in figure 13.

Figure 13: Reference structure.

To create acoustic models of the reference structure, the grids on both ends of the cylinder were omitted as their contribution to vibrational characteristics were estimated to be small. The rounded corners of the access hatch were modeled at right angles.

Main dimensions of the reference structure are presented in figure 14 and collected to table 2. Bulkheads divide inside of the cylinder to three compartments. Ballast tanks are located on the both ends of the structure. Space for instrumentation is located in the middle with a watertight access hatch on top, at the bottom of instrumentation cavity is a T-beam with the same length as the cavity and the webs with length of 150 mm. The reference structure had additional support attached to the outside of the shell below both inside bulkheads, not presented in the figure 14, but visible at figure 13. These supports were at line with the inside bulkheads. Instead of ballast tanks, additional weights were installed on outside bulkheads. All components of reference structure are manufactured from stainless steel EN 1.4301. Main material properties are listed on table 2. Averages

of minimum and maximum values provided by CES Edupack (2015) are used in the model.

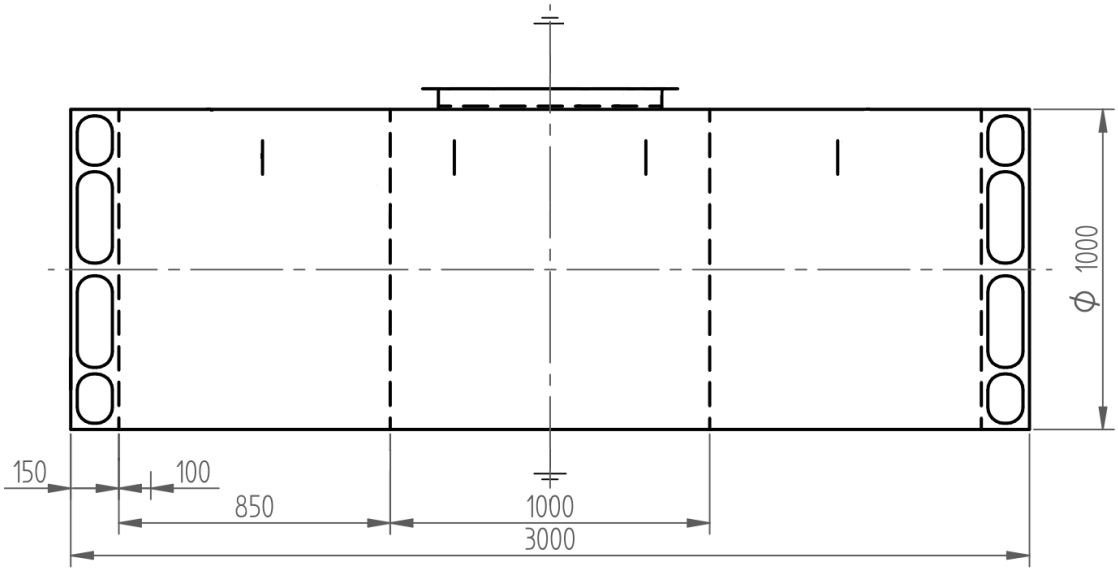

Figure 14: Main dimensions of reference structure, dimensions in millimeters.

	Symbol	Value
Lenght of the stucture (exluding grids) (m)	L	2.7
Outside diamiter (m)	D_1	1
Inside diamiter (m)	D_2	0.85
Thicness of end bulkheads (m)	h	0.01
Thicness of inside bulkheads (m)	h_2	0.005
Elastic modulus (GPa)	E	196.5
Shear modulus (GPa)	G	77.5
Density (kg/m^3)	ρ	7955

Table 2: Main dimensions and material properties of the reference structure, excluding grids and manhole. (Granda Design Limited, 2015)

5.2 Analytical model of the reference structure

Modal response of the reference structure is approximated using beam and shell equations to calculate natural frequencies $\omega_n \quad n \in [1,10]$. In this work the solution is calculated for dry structure. Beam equation is presented in equation (8) and equation for cylindrical plate in equation (10). The free body diagram of the beam problem is presented on figure 15.

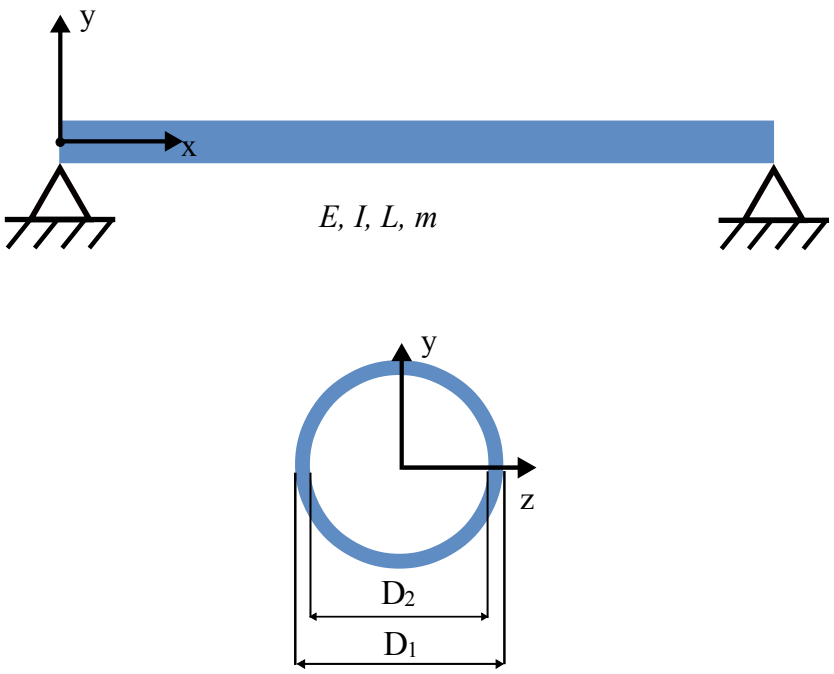

Figure 15: Free body diagram of the simplified reference structure.

Material properties and dimensions are in the table 2. Mass per unit length is written using density ρ and area A, as presented in equation (45).

$$m = A\rho \tag{45}$$

Second moment of area for a circular cross section is calculated using equation (46). (Santaoja, 2009, p. 197)

$$I = \frac{\pi}{64}\left(D_1^4 - D_2^4\right) \tag{46}$$

Eigenvalues λ^2 of equation (10) are provided for stiffly supported cylindrical plates, the values are presented in table 3. The plate has zero nodal circles inside the plate. Modal densities are calculated using equation (11) for one third octave band bandwidths presented in table 1.

n	λ^2
0	10.2158
1	21.26
2	34.88
3	51.04

Table 3: Eigenvalue solutions to circular plate natural frequency equation with zero nodal circles (Leissa, 1969).

5.3 Statistical energy analysis model of the reference structure

SEA model is a simplification of structure presented on figure 14. SEA model of the reference structure was created using shells, beams acoustic cavities and junctions. The same model is used as basis for the FEM model, thus it is divided on water line. Shell elements are divided to smaller elements around the measurement locations to provide small area where the vibration is approximated. Recorded response converted to one third octave band was imported to VA One and used as a force in the model. The point force was located on the beam at the bottom of the instrument cavity. The direction was to *y* direction in the global coordinate system. The SEA model presented in figure 16.

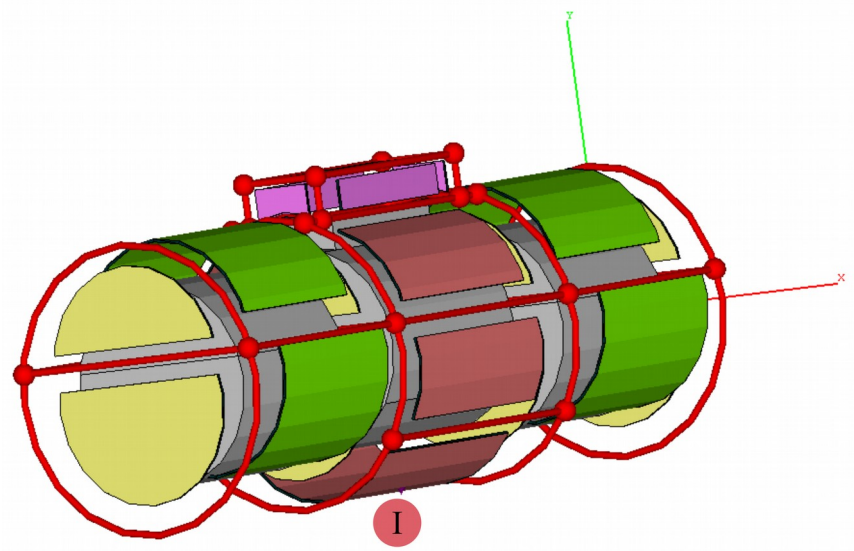

Figure 16: Exploded view of SEA model of the reference structure. Acoustic cavities are gray, beam in light blue, plates are in green, yellow and brown. Point and line junctions are red. Light red dot I marks location of point force. Axis z is from right to left, to the inside of the structure.

The SEA model was solved in VA One using AutoSEA2 solver. In SEA model, one element has only one degree of freedom, energy. Elements may be very large without the loss of accuracy. By comparison, in finite element model structural subsystems are divided to small elements and every element has multiple nodal degree of freedom. Fewer degrees of freedom reduces computational load of SEA model significantly, in comparison to FE model.

5.4 Finite element model of the reference structure

FE model is a simplification of structure presented on figure 14. Model is created from SEA model presented in chapter 5.3 by converting SEA acoustic and structural to corresponding FE elements. SEA junctions were replaced with FE junctions and FE faces. Structural FE model was created using quadrilateral plate and beam elements. The model is divided on water line and a FE face is added to outside shell elements below waterline. From the image of FEM model the weakness of FE generation algorithm in VA One is visible. To produce quality results, the mesh should be uniform and use only square elements. Due to limitations in meshing algorithm of VA One, outside shell elements were divided at waterline. Used element length $d_{element}$ is $d_{element} \approx 0.03\,\mathrm{m}$ that corresponds to factor n=6 in equation (44) in a frequency range to 1000 Hz. Structural FE model used in the thesis is presented on on figure 17.

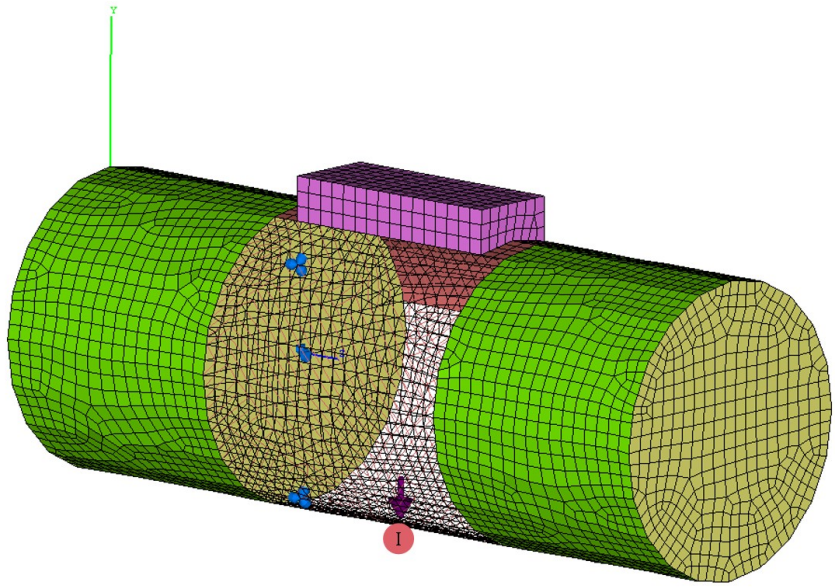

Figure 17: Structural FE model of the reference structure using factor 6. Structural elements shown in green yellow and red. Sensors are blue dots, corresponding to measurement locations #113, #178 and #179. Light red dot I marks location of point force. Axis x is from left to right.

Finite element model was solved in VA One using COSMIC NASTRAN solver. First six rigid modes provided by FEM analysis are ignored. The model has no border conditions, thus the first six modes are not real rigid modes. Real global modes occur at higher frequencies. This is applied to data by filtering response below 16 Hz. The velocity response is recorded using thee sensors, one for each three dimensional coordinate dimension, in each of locations #113, #178 and # 179. Locations of sensors are collected in table 4. Positive direction of sensors are the same as positive directions of accelerometers presented in chapter 6.2.

Number of sensor	*X*	*Y*	*Z*
#113	0.76×10^{-3}	-0.49	-0.85
#178	0.42	-0.77	-1.09
#179	0.43	-0.26	-1.12

Table 4: Location of sensors in X, Y, Z coordinate system. Origin is at the highest node on global structural Y axis. Global structural coordinate system is fixed on the center of the outside bulkhead closest to measurement location in inside bulkhead.

All cavities inside the structure were modeled using acoustic triangular FE acoustic elements. Acoustic model is connected to structural model using FE faces. Acoustic model of inside cavities is presented on figure 18. All cavities were filled with air with the temperature of 5°C.

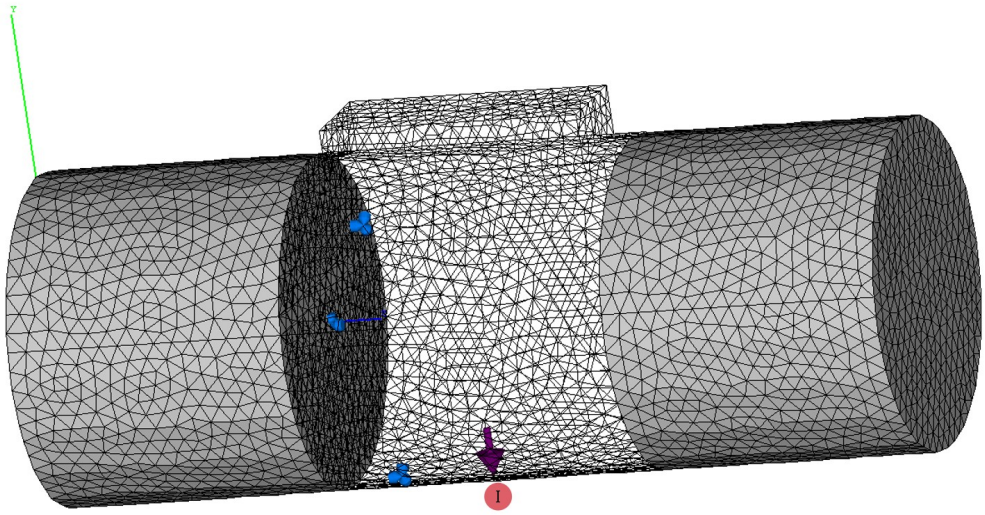

Figure 18: Acoustic FE model of the reference structure using factor 6. Acoustic elements shown in gray. Sensors are blue dots, corresponding to measurement locations #113, #178 and #179. Light red dot I marks location of point force. Axis x is from left to right.

6 Measurements

6.1 General arrangements

As part of this thesis, sea trials were conducted in Brattnäs sund in Pargas, Finland on 25th November 2015 between 06:30 a.m (UTC) and 14:00 a.m. (UTC). During the measurements the air temperature was 6 °C and air pressure 100,5 kPa. Winds were high and there was light rain. (World Weather Online, 2016)

Location of the measurements was a sheltered strait in the inner islands of Archipelago Sea. The coordinates of the reference structure during measurements were 60°16,190'N and 22°19,126'E (WGS84). Approximate location of the reference structure during the measurements is presented on the map presented on figure 19. Depth contour lines and depth points are also presented on the map.

Figure 19: Location of the sea trials of the reference structure in Pargas, Finland . Displaying depth contour lines and depth points. (Map provided by: National Land Survey of Finland, 2015)

Measured water depth during measurements at Brattnäs sund is 10 m. Compared to floating position of the example strcture, water was deep. Water line was approximately 10 cm over center line. Floating position of the reference structure during sea trials is presented on figure 20.

Figure 20: Floating position of reference structure during sea trials.

The dry structure was supported on straps, presented in figure 21, during the measurement of response of dry structure to sine sweep. Forced response was measured when the structure was loading in water, as presented in figure 20. During the measurement of forced response, the monitor boat was anchored clear from the reference structure with engine shut down.

Figure 21: Reference structure during measurement of response of dry structure.

Density, salinity, and temperature of the sea water were measured using Castaway CTD instrument. Averages of measured values over water depth were collected to table 5. Other required thermal constants for water are calculated by using methods introduced by Sharqawy et al. (2010) Air temperature was measured using Slam Stick. The speed of sound in the air was calculated using equation (47) (Zuckerwar, 1997, p. 62). Other properties for air are provided by VA One. Used properties for water and air are presented on table 5.

$$c = \sqrt{\frac{\gamma P}{\rho}} \tag{47}$$

	Sea water proparties during sea trials	Air proparties during sea trials
Density (kg/m$^{3)}$	1440.40	1.2256
Speed of sound (m/s)	1140	334.319
Salinity (g/kg)	10792.11	N/A
Temperature (°C)	6.50	5
Specific heat ratio	1.01	1.4
Dynamic viscosity (μN s/m$^{2)}$	1460	17.83
Kinetimatic viscosity (μm^2/s)	1.02	14.55
Molar mass (g/mol)	18.078	28.965
Prandtl Number	10.465	0.71
Specific gas constant (J/kg K)	N/A	287.05

Table 5: Thermal and chemical properties of water and air during sea trials. Water density, salinity and speed of sound are averages over the depth of the water. (Franklin, Suckow and Weisbroth, 1995; Dixon, 2007)

6.2 Measuring response

All instruments were located at the instrumentation space inside the structure. The response of the structure was recorded using three Slam Stick X accelerometers, recording acceleration on three axis, pressure, and temperature. Sample rate of the sensors was 4994 Hz. Acceleration range for accelerometer at location #113 was $\pm 100\,\mathrm{g}$. Measurement range for accelerometers at locations #178 and #179 were $\pm 25\,\mathrm{g}$. Accelerometers were located to have one sensors below water line, one above waterline in the outside shell and one in the outside bulkhead. Initial FEM analysis was used to decide the location of sensors. Location of accelerometers is presented of figures 22 and 23. Positive coordinate systems for measurements locations are also presented in figure 22.

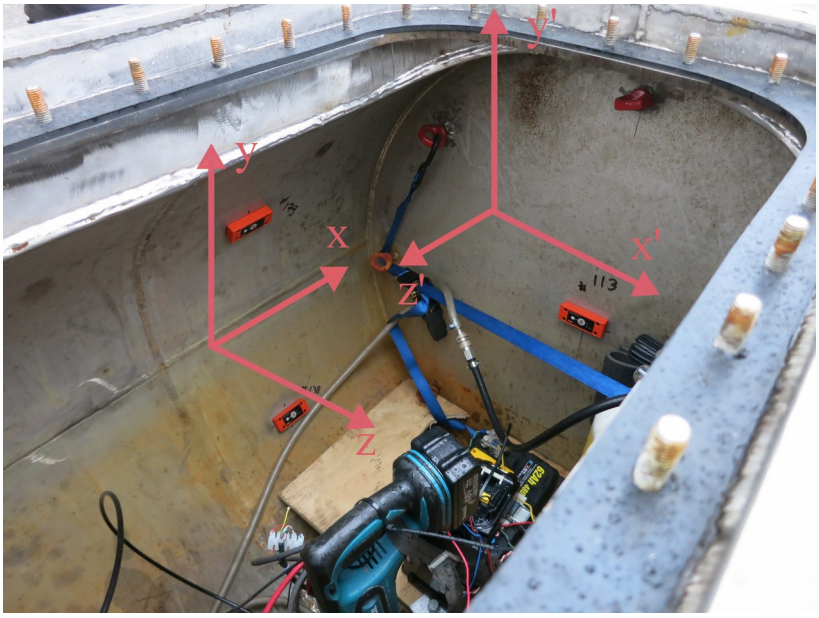

Figure 22: Location and positive axis of acceleration sensors used in sea trials. Coordinate system x', y', z' is local to measurement point #113. Coordinate system x, y z is local to measurement points #178 and #179. Sensors are orange boxes.

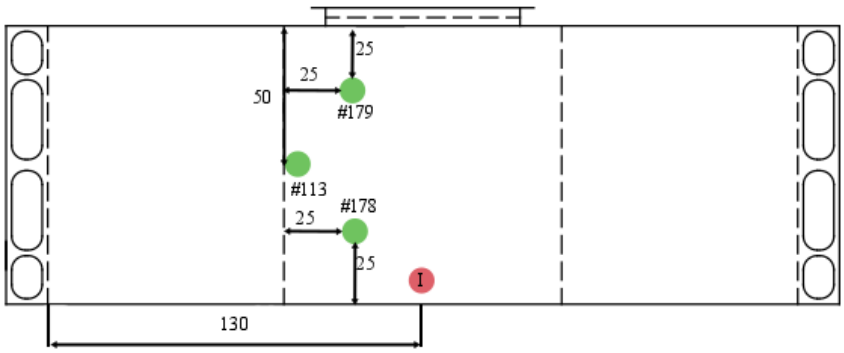

Figure 23: Measurement and exaction points on reference structure used in modeling and sea trials. Shock vibration at point I, sensors at points #113 and #178 and #179. Dimensions are in centimeters.

Analyzing software for Slam Stick provided time-acceleration data with a possibility to convert to frequency-acceleration domain using fast Fourier transform. An GNU Octave code was created to read comma separated value (CSV) data from measurements and calculations performed using VA One and to convert the measured signal to one third octave frequency band before displaying and saving figures. Acceleration data was converted to velocities using relationship between velocity v and acceleration a, presented in equation (48).

$$v = \frac{a}{2\pi f} \tag{48}$$

6.3 The impulse

The structure was excited with acoustic impulse and shock impulse. Acoustic sound source was hung using straps inside instrument cavity, shock impulse impacted the bottom of instrument cavity. Before tests on water loaded structure, the dry structure hanging from straps was excited from outside with a hammer and sine sweep to measure natural frequencies. Modal response of the dry structure was measured to verify modal solution and the acceleration measurements. Striker used to generate the shock impulse was located on the t-beam, presented in figure 24. The impulse force source was mounted on spar of T-beam at the bottom of instrumentation space. Force sensor was attached to the web of the beam. The draft of the mounting arrangements is presented on figure 24.

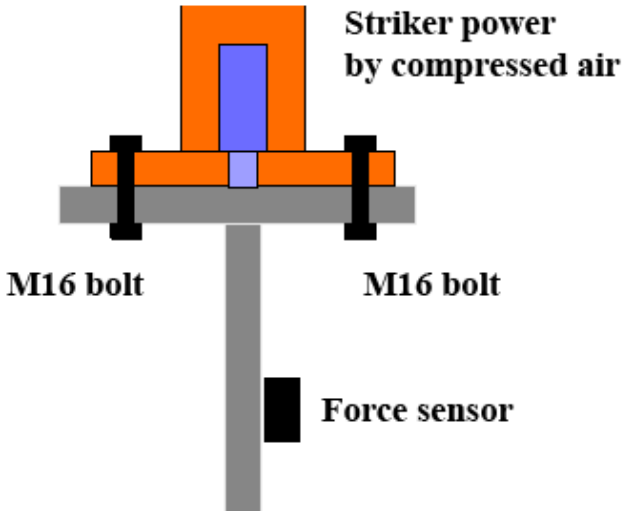

Figure 24: Draft of mounting of shock impulse device and force sensor on the T-beam.

The shock source used on water loaded structure was operated using remote control. The structure was excited with an audio sweep, sine sweep, to record modal response and to have comparison between dry and water loaded situation. Sine sweep was played continuously, first 0.3 s the sweep were used in the comparison.
General arrangements of the shock impulse sources inside instrumentation space are presented on figure 25.

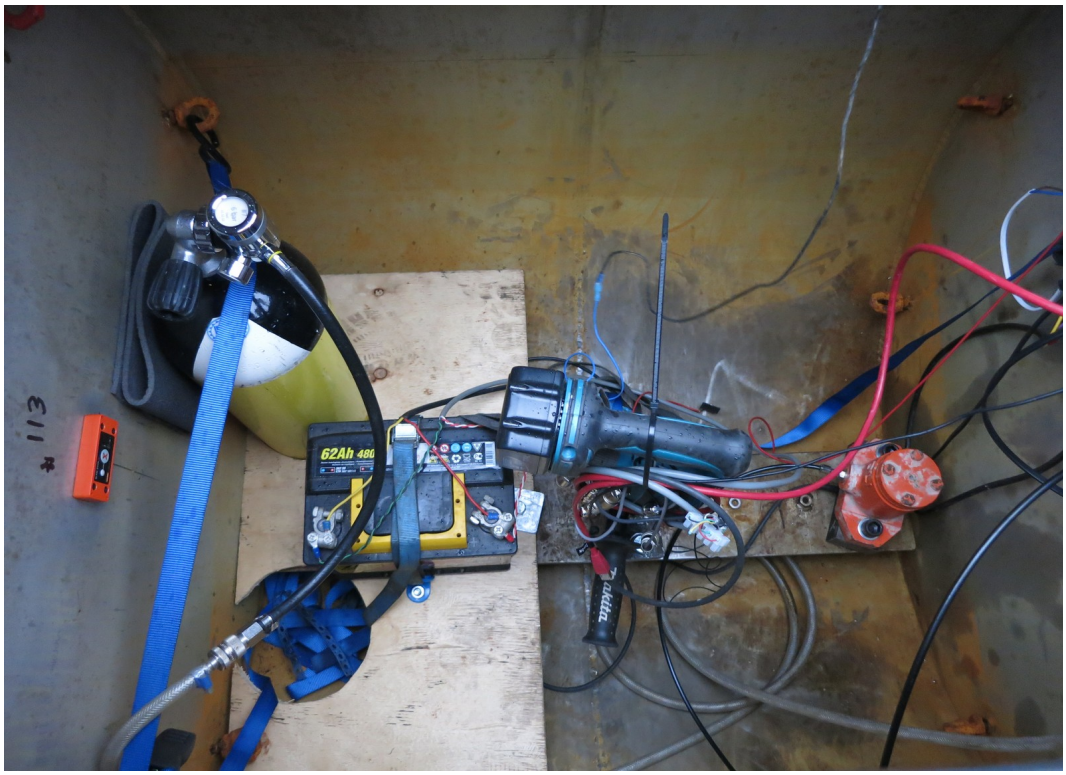

Figure 25: General arrangements at the bottom of instrumentation space. Shock impulse source is visible on the right side of the image.

Forces were recorded using sample rate was 1000 Hz, setting the maximum frequency of the measurements. Used force sensors were Kyowa LMB-A-500N and Kyowa LMC-A-5KN-P 5kN. A GNU Octave code was used to read the recorded data and convert it from time-force domain to frequency–force domain using fast Fourier transform. The program by Jaouen (2011) was used to convert it to one third octave bans. Converted signal was saved as CSV file format to use in VA One.

At the lowest frequencies, the force is 100 N, after 20 Hz the force stabilizes to range between 20 and 30 N. Time domain representation of shock impulse, recorded on the outside shell, shows the *x* component of the shock impulse. Impulse on other components was out of the range of the accelerometer. The measured force on one-third frequency domain and on time domain are presented on figure 26.

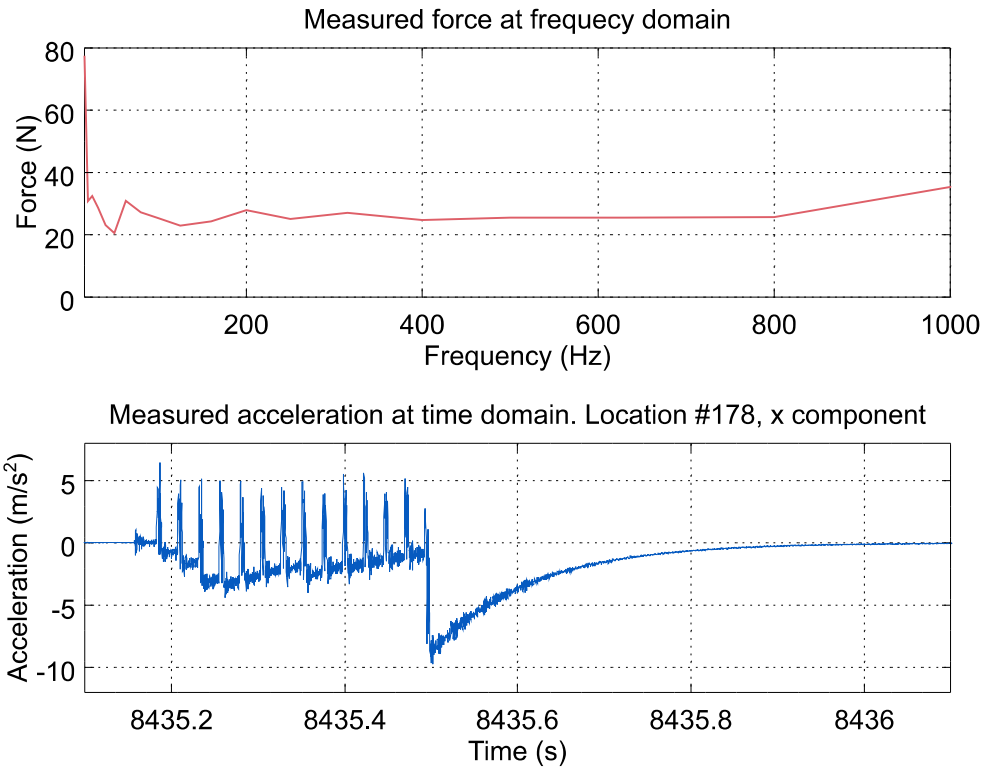

Figure 26: Measured force in frequency domain, on ⅓ octave bands, and measured acceleration in time domain in the outside shell, between 10:18:40.4 a.m. and 10:18:41:3 a.m. (UTC).

7 Analysis of results from calculations and sea trials

The quality of measured results is assessed by comparing narrow band velocity–frequency graphs to typical features of vibrational response in low, mid, and high frequency range. In low frequencies, the response graph exhibits well separated response peaks, in high frequencies, the response graph is smooth, no clear peaks are distinguishable from from the response spectra. In mid frequencies, the response peaks are visible but not well separated. A graph with sufficient quality should have at least low and mind frequency ranges present. (Soize, Desanti and David, 1992, chap. 2.5)

Calculation of modal properties for dry structure is supported by strong theory, so modal properties measured and calculated for the structure are studied in detail to validate the finite element model. Effect of water loading is studied by comparing response to sine sweep in a location with direct contact to water and inside bulkhead.

Low frequency range of forced response is searched from plots of narrow band response of forced response using definition by Soize, Desanti and David (1992). Response calculated using finite element method and measured response are compared in this low frequency ranges. Statistical energy analysis is compared on whole frequency range to assess suitability to modeling in low frequency range.

The structure was excited multiple times and the impulse source was kept for few seconds. Slam Stick Lab provided measured acceleration in time domain. From plotted measured acceleration graphs, a representative acceleration peak was chosen, studying data from the location #178, where the impulse is measured most directly. Suitable acceleration peak is to be separated from other peaks and the surrounding peaks are similar. The results are converted to frequency domain using fast Fourier transform tool in Slam Stick lab. Converted measured accelerations and plotted against results. Two different acceleration peaks and corresponding force data were tried, without effect on results The data is exported from Slam Stick Lab using CSV files. GNU Octave codes were created to analyze the results.

Measured and modeled modal densities were calculated using equation (11). Results were plotted using GNU Octave. In the code the results of forced response test were converted to one third octave bands using a GNU Octave code created by Jaouen (2011) in conversion of narrow band response to one third octave band. The magnitude of vibration, $\bar{x}$ was calculated from measurement data of x, y and z components using equation (49).

$$\bar{x} = \sqrt{x^2 + y^2 + z^2} \tag{49}$$

Flow chart of GNU Octave code used to analyze the results of test of modal response is presented in figure 27 a). Flow chart of GNU Octave code used to analyze the results of forced response is presented in figure 29 b).

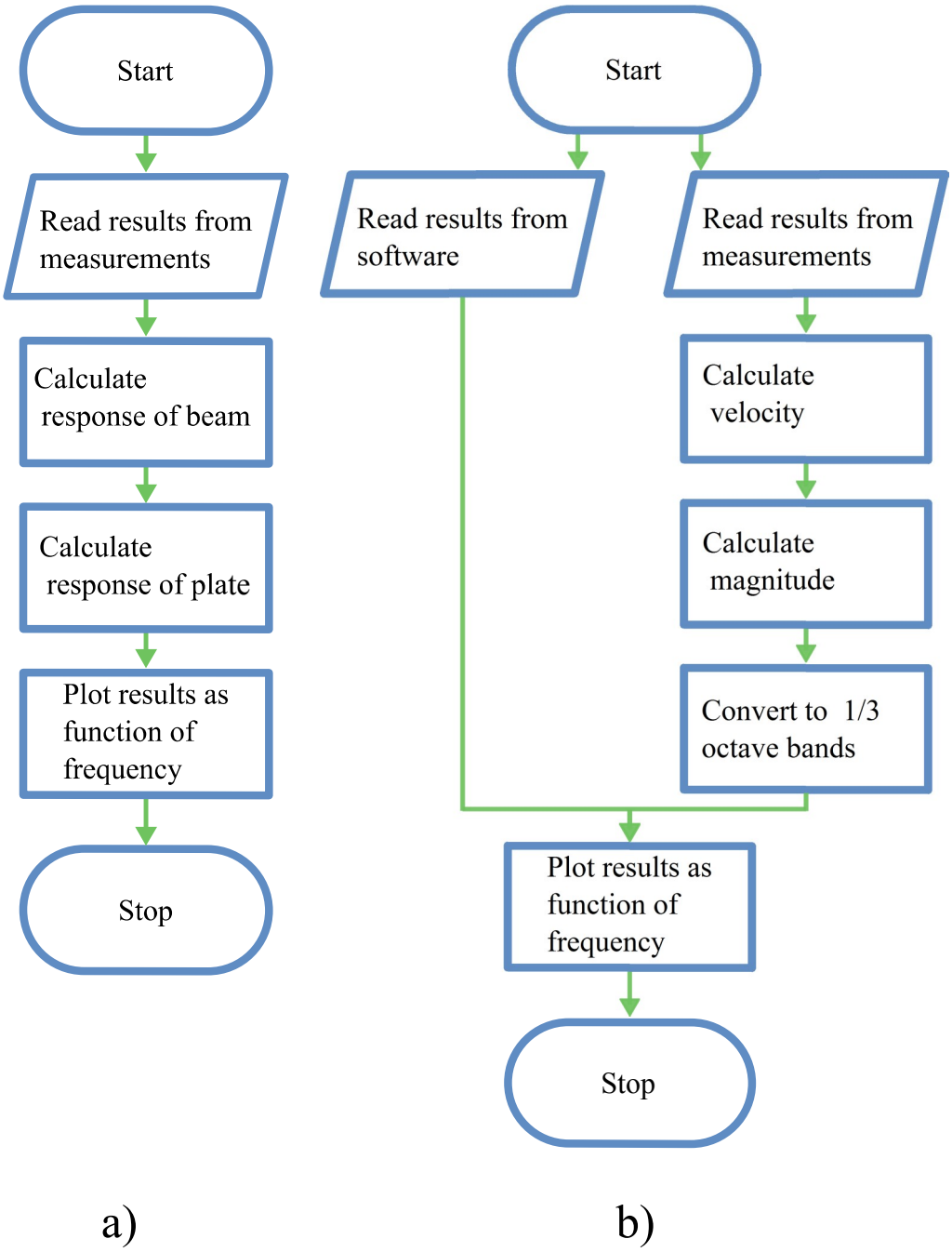

Figure 27: Flow chart of GNU Octave code used to analyze the modal response in figure a) and forced response in figure b).

8 Results

8.1 Introduction

During sea trials, the dry structure was excited separately with a hammer and an acoustic impulse. In this chapter, modal properties are studied using calculations performed using analytical plate- and beam theories. The calculations performed using finite element method and analytical methods are compared to measured modal properties. Also the effects of water loading to modal solution are studied using the measured response of dry and water loaded structure to sine sweep.

Forced response is studied to provide understanding on final part of the transfer of vibration from machinery to water. Responses measured in two locations and on three directions at each location are compared to calculations performed using finite element method. Measurement of forced response in location #178 failed because response was greater than measuring range of the accelerometer. Components of measured response are summed to provide magnitude of the response. The magnitude of the response is compared to average velocities calculated using statistical energy analysis for elements surrounding the measurement location.

8.2 Modal properties of dry structure

The values for the first frequencies were calculated using analytical methods presented in chapter 5.2. For plate, first six were in the frequency range of this work. For beam, first ten natural frequencies were in the frequency range. Calculated natural frequencies are presented in table 6.

Mode number n	Beam (Hz)	Plate (Hz)
1	11	12
2	44	50
3	100	135
4	178	289
5	278	539
6	400	915
7	544	
8	711	
9	900	
10	1111	

Table 6: Natural frequencies calculated using analytical methods

In frequencies greater than 500 Hz the vibrational behavior is global, as illustrated in figure 34. Mode shapes at low and high frequency are compared at figure 28. At 180 Hz, the vibration is local, this results vibration only in the outside bulkheads. At 500 Hz, vibrational behavior is global, presenting horizontal vibration corresponding to vibration of beam. In higher frequencies, such as 500 Hz assumptions used to provide analytical solution to modal analysis are not valid. This corresponds to typical vibrational behavior at specified frequency ranges.

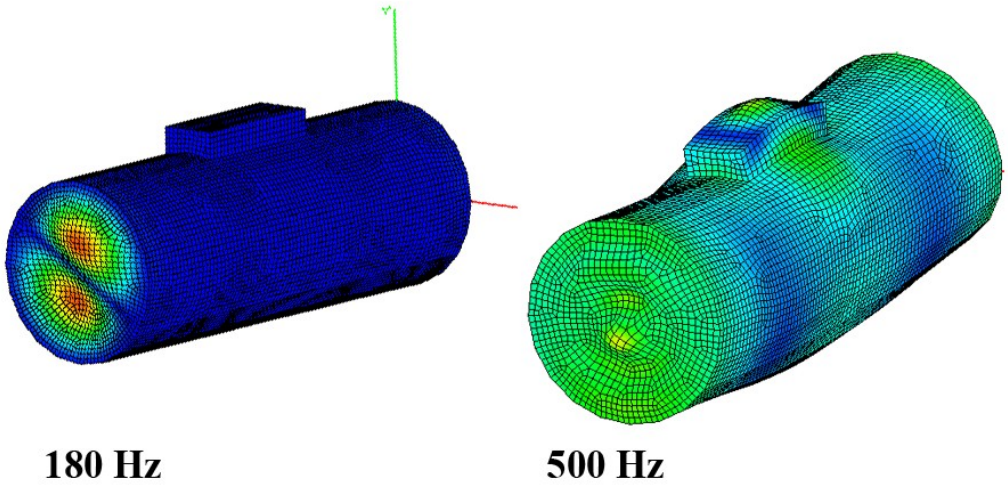

Figure 28: Modes of vibration of the reference structure at low frequency, presenting local vibration and at high frequency, presenting global vibration.

The dry structure hung from straps was excited with a hammer to determine the natural frequencies and the modal solution of dry FE model of the reference structure was analyzed without water loading to validate the FE model.

FEM analysis of VA One does not provide exact natural frequencies, instead it calculates natural frequencies around the center frequency. The natural frequencies calculated using FEM were collected to one third octave bins. Also the modal density of FEM model was calculated from the bins. VA One calculated natural frequencies at bins centered at 100 Hz, 250, 315 Hz and 400 Hz. At binds centered around 125 Hz, 160 Hz and 200 Hz were no natural frequencies. After 250 Hz, the upper band limit corresponds to lower limit of the next band. Center frequencies and upper and lower limits of one third octave bands studied in this work are presented in table 1.

To verify FE model, every natural frequency bin calculated using FEM should have at least one corresponding measured natural frequency. The measured natural frequencies are indicated by peaks at measured acceleration response. On outside shell, the measured natural frequency at 100 Hz corresponds to calculated natural frequency bin centered at 100 Hz. The measured natural frequency at 180 Hz does not have a direct measured equivalent on the inside bulkhead, but it is close to the lower band limit of band centered at 250Hz. There is a minor natural frequency in the outside shell and inside bulkhead at 250 Hz corresponding to the calculated bin centered at 250Hz. The calculated bin centered at 315 Hz corresponds to measured natural frequency at 320 Hz. The calculated bin centered at 400 Hz does correspond to natural frequency measured on the inside bulkhead at 380 Hz. These calculated FE natural frequency bins with corresponding center frequencies and upper and lower band limits are plotted on figure 29 against measured acceleration response in the inside bulkhead and outside shell.

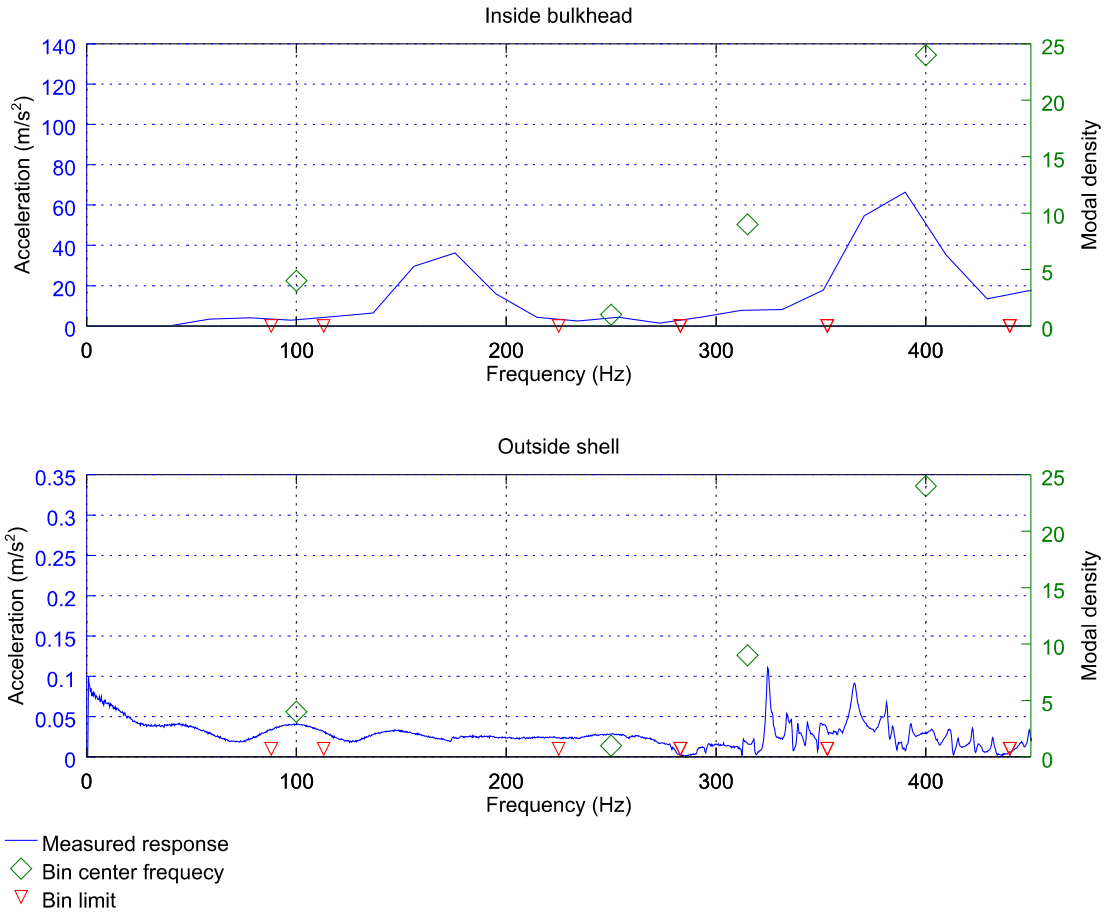

Figure 29: Natural frequencies calculated using FEM and measured natural frequencies compared. Measured narrow band response in blue, center frequencies of one third octave bands and corresponding modal densities in blue and upper and lower boundaries of one third octave bins in blue.

In higher frequencies analytical methods fail to predict natural frequencies, as is illustrated in figures 35 and 30. The plot of response of the outside shell below water line, location #178, illustrates the typical behavior of low, mid and high frequency ranges. After 1000 Hz, the response is typical to high frequencies, no clear peaks are visible and the acceleration stabilizes as frequency increases. Between 300 Hz and 1000 Hz, the behavior is typical to mid frequency range; acceleration peaks are visible, but not well separated. Below 300 Hz, the frequencies are well separated, indicating highly modal behavior. Natural frequencies calculated using analytical methods illustrate close agreement at 50 Hz, after 50 Hz natural frequencies of a plate does not correspond to measured natural frequencies. Measured natural frequency at 100 Hz corresponds to beam natural frequency at 100 Hz. After 100 Hz beam natural frequency does not correspond to measured natural frequencies. and circular shell natural frequency at 177 Hz. After combined natural frequency at 150 Hz the analytical methods fail to predict the natural frequencies. Plot of response at outside shell, below waterline location #178 is presented on figure 30.

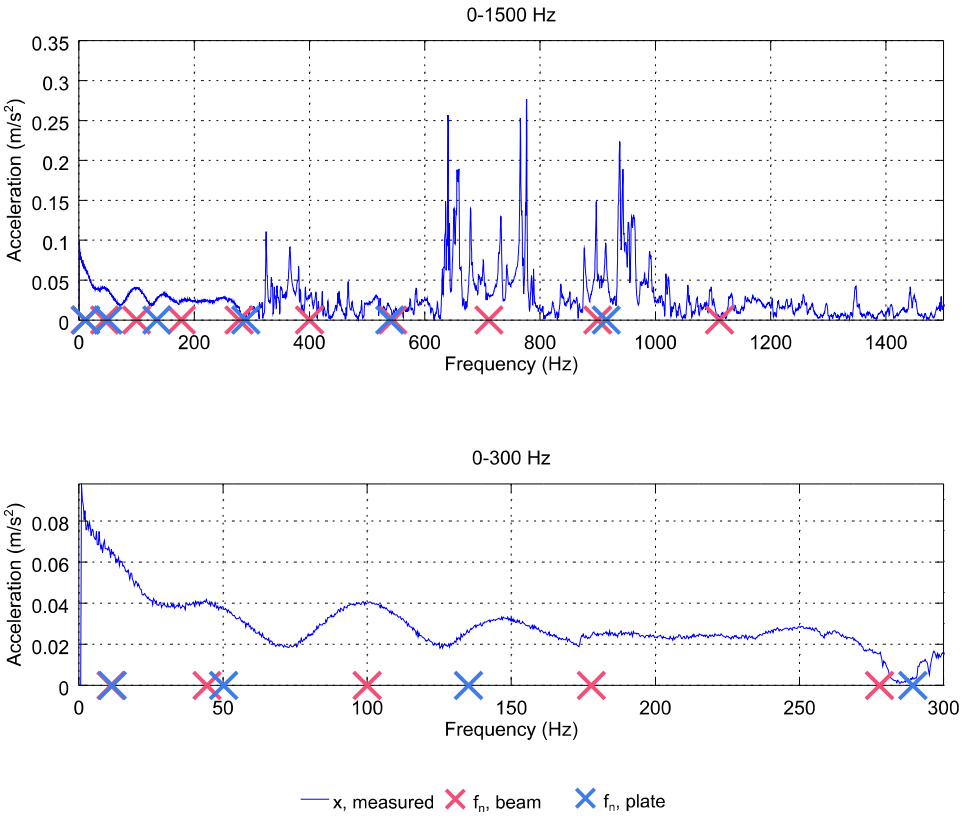

Figure 30: Measured narrow band response of dry reference structure to high frequencies compared to analytically calculated natural frequencies for circular plate and beam. Response at inside bulkhead and outside shell, below water line.

8.3 Effect of water loading

The effect of water loading to modal behavior was studied in two locations. In the location #113, located in the inside bulkhead, water loading does not change the natural frequencies. This demonstrates low damping effect of the water in the inside bulkhead.

For measurement location above water line in the outside shell, the effect of the water loading is significant, reducing the major natural frequency from 300 Hz to150 Hz. Vibrational acceleration to *z* direction, outside of the shell, at the natural frequency is significantly reduced as is acceleration in horizontal direction. Acceleration in vertical direction, component *y* is increased. Maximum acceleration at the major natural frequency is reduced on all components. The phase of the natural frequency at locations and #179 at the first natural frequency at 30 Hz, is changed. Response to sine sweep in both locations and for dry and water loaded structures are presented in figure 31.

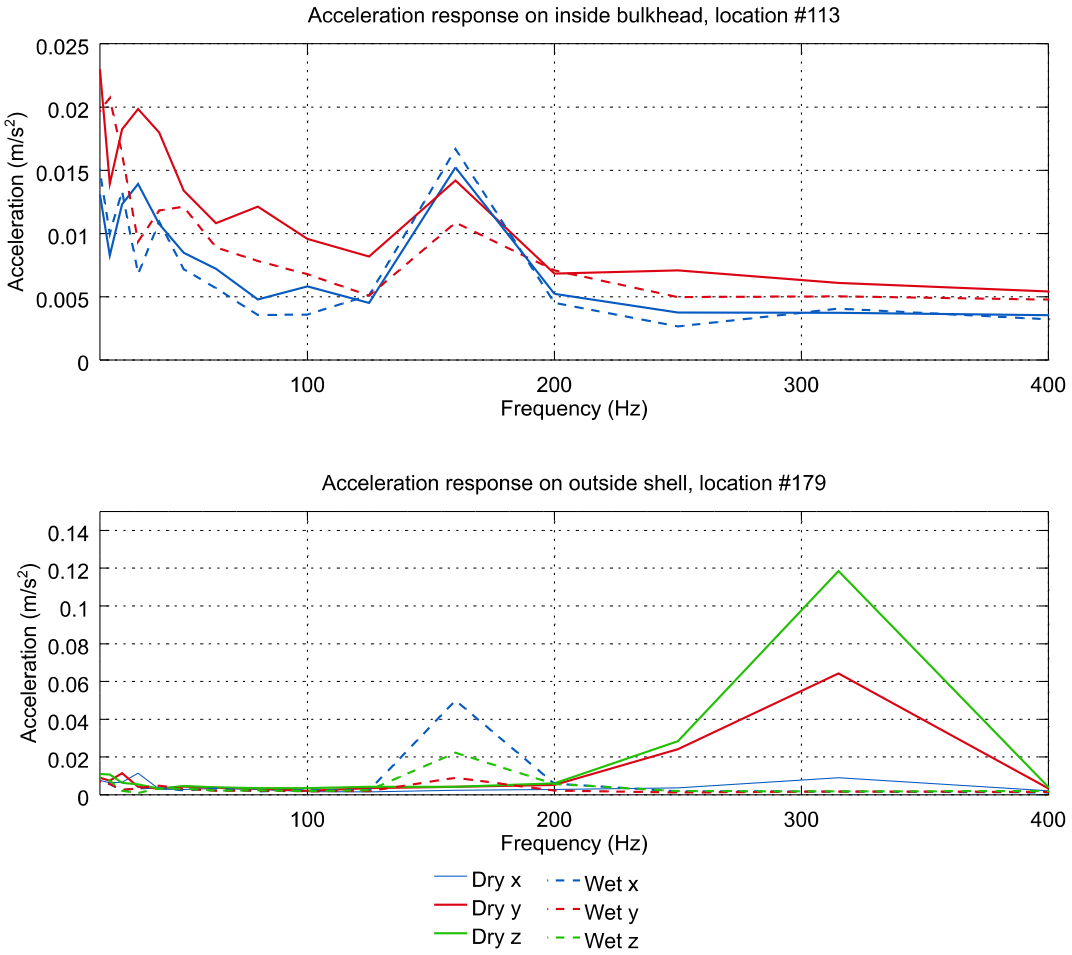

Figure 31: Response of reference structure in ⅓ octave bands. Dry and water loaded structure compared on inside bulkhead and outside shell.

8.4 Forced response

8.4.1 Global response

The contour plot of the response at the resonance frequency of 160 Hz is calculated using FEM. The plot displays locations of the measurement sensors in reference to local velocity peaks. Accelerometers were positioned near local velocity peaks, but not at the location of maximum acceleration. Contour plot produced by VA One for forced response using measured response is presented in figure 32.

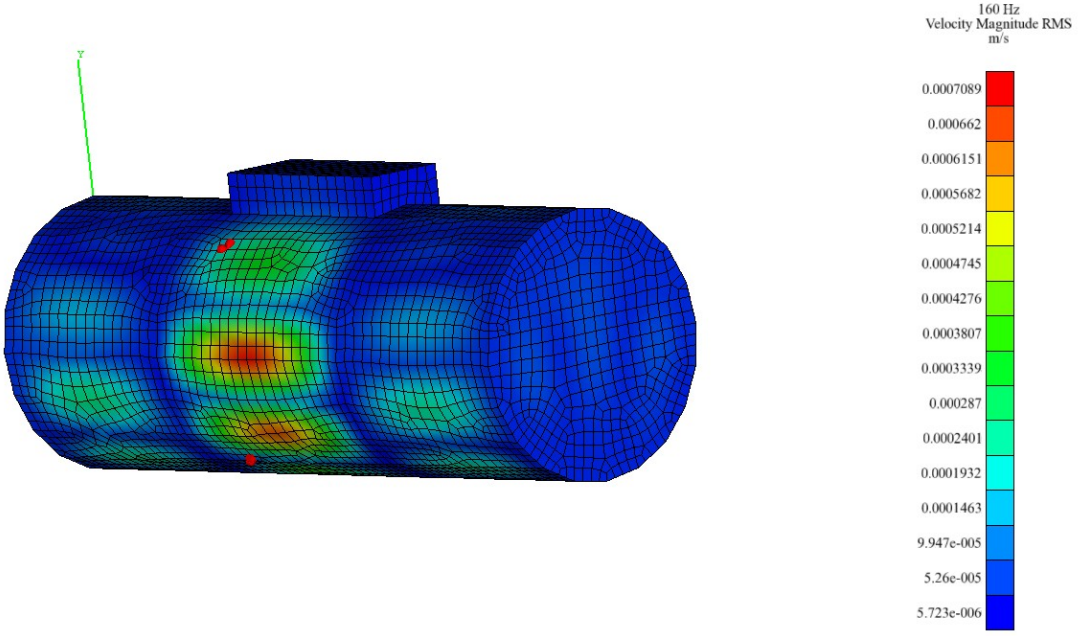

Figure 32: The contour plot of response at resonance frequency of 160 Hz is calculated using FEM. Red dots represent locations of the sensors.

8.4.2 Statistical energy analysis and measurements compared

In the inside bulkhead on the location in the outside shell the measurements failed due to high accelerations. On measurement point located above water line in the outside shell, the measurement succeeded. The magnitude of measured narrow band response exhibits typical low frequency range characteristics to 200 Hz and typical mid frequency range characteristics to 600 Hz. After 600 Hz vibration is typical high frequency vibration. Response calculated using SEA follow the general trend of measured magnitude. The calculated response omits the peaks of measured response because SEA calculates average over all possible results. Results calculated using SEA follow the general trend of measurements. The velocity level is higher, as predicted by the theory. The accuracy of SEA increases as frequency increase, but even in low frequencies response calculated using SEA is accurate enough for first predictions. The magnitude of measured narrow band vibration and the magnitude of measured response is compared to results calculated using SEA are presented in figure 33.

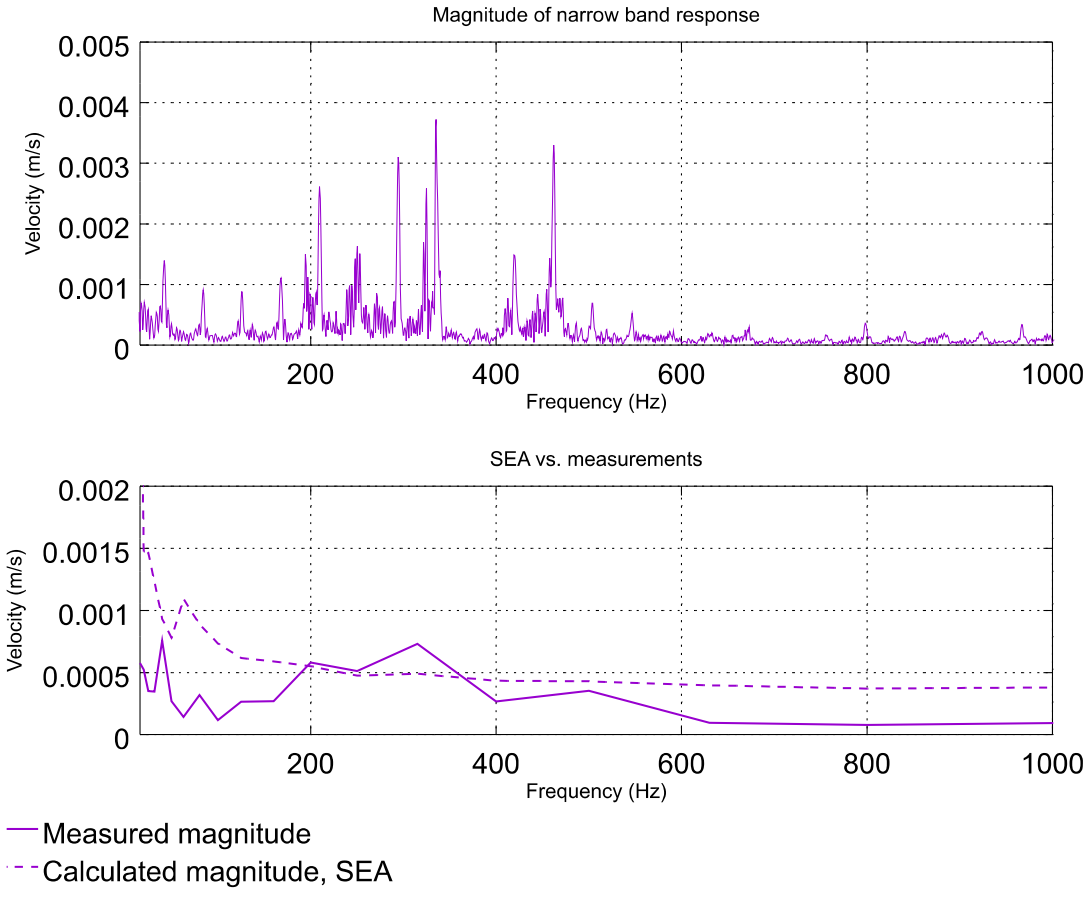

Figure 33: Measured magnitude of narrow band response to shock impulse and measured and response calculated using statistical energy analysis compared at ⅓octave bands. Location #179 on the outside shell

8.4.3 Finite element analysis and measurements compared

Response to forced response was recorded in three locations. The locations and positive directions are presented in figures 22 and 23. On the inside bulkhead and location closest to source measured accelerations exceeded the range of accelerometers. In the inside bulkhead measurements of *x* and *y* components succeeded, *z* component failed because of high accelerations. Failure in *z* direction is caused because inside bulkhead does not have vibrational damping from the surrounding water in the same level as in the other measurement locations. This causes inside bulkhead to have highest vibrational levels.

Below 200 Hz measured response of *x* component in inside bulkhead location #113 does not have evident resonant frequencies. Above 200 Hz natural frequencies are well separated. Between 200 Hz and 1000 Hz response difference between measurements and calculation is caused by difference of measured natural frequency at 300 Hz. Natural frequency predicted by FEM is at 250 Hz. Another measured natural frequency 500 Hz does not occur in FE model. Despite these differences, the response obtained using FEM follow the general trend of measured response.

Study on low frequency response of *y* component of inside bulkhead location #113 in narrow frequency band, exhibits natural frequencies at 40 Hz, 80 Hz, 120 Hz and 170 Hz. After 200 Hz the response spectra is typical of mid frequency range. Measured response has natural frequency at 40 Hz not present in response calculated using FEM. Omitting this difference, the response calculated using FEM follows the general trend of measured response.

Below 400 Hz measured narrow band response of *x* component in outer shell above water line, in location #179, has characteristics of typical low frequency range. Above 400 Hz the response is typical of the mid frequency range. Below 200 Hz FE failed to calculate natural frequencies. The natural frequency at 200 Hz was calculated correctly using FEM. The calculated natural frequency at 250 Hz was 50 Hz off the measured natural frequency. Response calculated using FEM follows the trend of measured response, with difference of 50 Hz.

Narrow band response of *y* component in outside shell, in location #179 displays response typical to low frequencies below 150 Hz. Between 150 Hz and 550 Hz the response is typical of mid frequency range. After 550 Hz the response is typical of high frequency. Below 150 Hz response calculated using FEM follows the trend of measured response, while omitting the natural frequencies.

Below 200 Hz measured narrow band response of *z* component in outer shell has characteristics of typical low frequency range. Above 200 Hz the response is typical of the mid frequency range. After 500 Hz the response is typical high frequency response. Below 200 Hz response calculated using FEM follows the trend of measured response, while omitting the natural frequencies.

Measurement of acceleration in measurement point below water line on the outside shell, location #178 failed due acceleration levels extending the measuring range of accelerometers.

Measured narrow band response on all locations and to all directions is presented in the figure 34. Comparisons between measured and calculated responses on all locations and to all directions is presented in the figure 34.

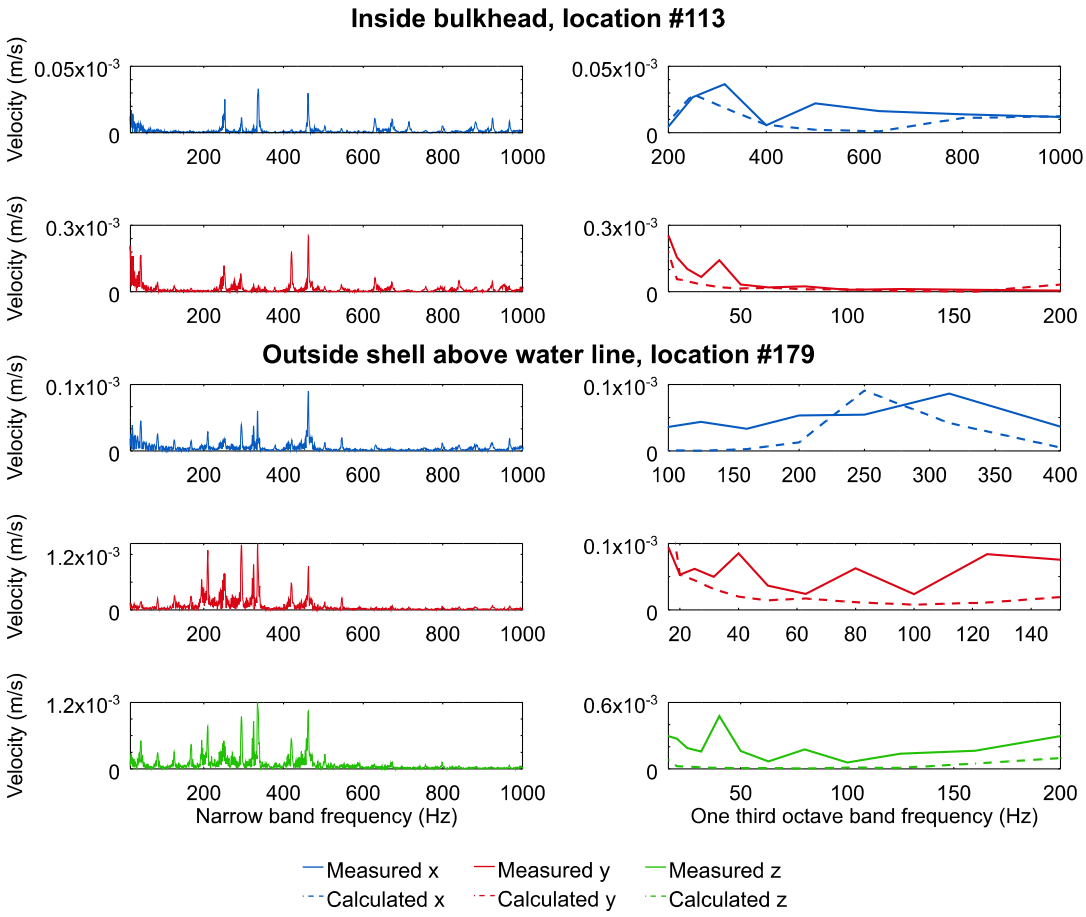

Figure 34: Measured narrow band response to shock impulse and response calculated using FEM and measured response compared on inside bulkhead and on outside shell above water line.

8.4.4 Finite element method and statistical energy analysis combined

FEM is considered by the literature to be suited to low frequency range and SEA to high frequencies. Between these two frequencies is the mid frequency range. For this range, hybrid methods combining elements from these two methods have been developed.

The measurements and statistical energy analysis at frequency range studied on this this work are presented in figure 35. Illustrative limits of frequency bands, presented by Cicirello et al. (2012) are reproduced in figure 1. In this work, the finite element model was solved to frequencies considered by Cicirello et al. to be at mid frequency range. Statistical energy analysis calculations of this work provided results with difference of one decibel on the whole frequency range, even in the mid and low frequency ranges. The maximum frequency studied in this work, 1000 Hz is the beginning of the high frequency range defined by Cicirello et al. It is the frequency range considered to be most suited to statistical energy analysis.

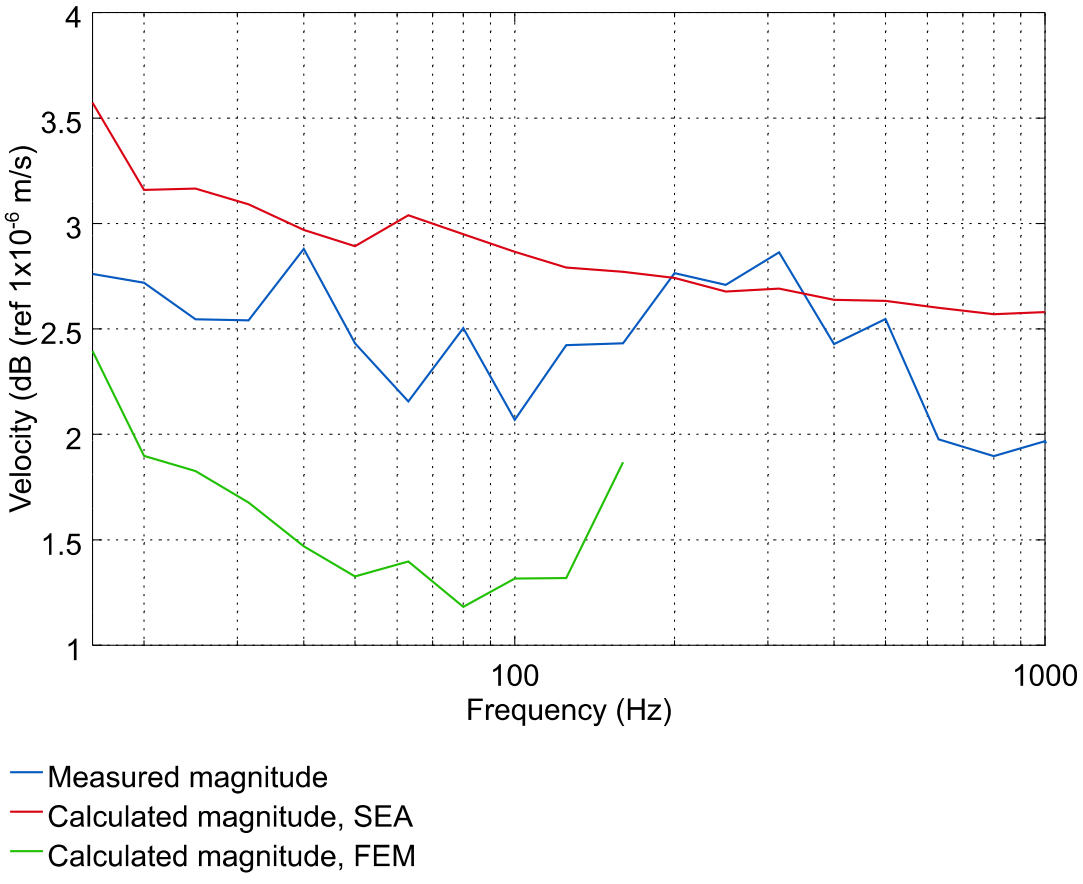

Figure 35: Measured response compared to response calculated using statistical energy analysis and finite element method. Location #179 on the outside shell. Frequency at ⅓ octave bands, with lowest center frequency at 16 Hz.

8.5 Concluding remarks

In this thesis, both measured and calculated modal behavior were observed to follow guidelines established by Soize et al. (1992). Low, mid, and high frequency ranges are visible in the plot of modal density and in the plot of response of the outside shell to high frequency range. Analytical equations of natural frequencies for beam and cylindrical plate provided results in the same range as measured natural frequencies. Natural frequencies calculated using finite element method were found to correspond well with the measured natural frequencies. Modal density of natural frequencies calculated analytically did not correspond closely to natural frequencies calculated using finite element method, but were close.

Comparisons of finite element method to the measurements of modal analysis indicate the finite element model to be correct, as measured and calculated resonance natural frequencies agree. Modal analysis also demonstrates the applicability of analytical equations to provide first estimates at a structure of this type. The natural frequencies calculated using analytical methods were higher than measured, this could be caused because shear is not included in the analytical equations.

In this study exclusion of water loading was observed to be possible to when studying components inside of the structure, as measured response results on the inside bulkhead, location #113, did not change when water loading was added. On other measurement locations, water loading had great effect on solution, as predicted by Ross (1987), by changing natural frequencies and damping vibration. Modal density was found to increase at a greater rate when water loading was added, demonstrating the necessity to calculate mesh density for submerged structure using the wave length of water.

The problem dominating all water loaded finite element solutions was found in this work to be inaccurate modeling of natural frequencies when structure was loaded with water. On all locations the measured trend of vibration followed the trend calculated using finite element analysis with small margin of error. The greatest error occurs at the natural frequencies. Finite element analysis assumes small displacements. In this thesis, measured accelerations were high, so the displacements may not be small at all locations and to all directions. This assumption may cause the error between measurements and displacements.

In chapter 8.2 of this work the finite element model was found to be correct using analysis of measured and calculated modal properties. In chapter 8.3 of this work effect of water loading on inside bulkhead location was found out to be small. Correspondingly, finite element method provided most accurate results in the inside bulkhead. Accuracy of results in water loaded measurement point on the outside shell was lower. Change of natural frequency between measured and calculated result is similar when comparing measurements on water loaded and dry structures. Thus the error is concluded to be caused by inaccurate modeling of water loading by wavelet method. In a study by Blanchet and Caillet, wavelet method was found to lose accuracy for improved computational speed in comparison to boundary element method (2012). Results obtained in this work confirm these results. When effect of water loading is

absent or modeled correctly and properties of finite element model match proprieties of frequency range, finite element method is capable to provide accurate results.

In this work, the analysis of results provided by statistical energy analysis were successful only in one location in the outside shell, location #179. In the other location on the outside shell the measurement failed. On inside bulkhead, one measured displacement components failed to provide accurate results, reducing quality of calculated magnitude of response. The results calculated using statistical energy analysis follow the measured response, with slightly higher level, smoothing response peaks by averaging nature of statistical energy analysis.

Comparison of response calculated using statistical energy analysis in the outer shell, location #179, confirm results calculated by Plunt (1980b) using statistical energy analysis to calculate response of a small scale model, without water loading. In the location #179 the results follow the general trend while omitting peaks, as observed by Plunt. Results obtained in this work were similar to results reported by Lu et al. (1982). They found statistical energy analysis to provide higher and averaged values when compared to measurements. This work achieved similar results, with improved accuracy. Yayladere and Çalışkan (2013) concluded in their study of submerged cylinder statistical energy analysis being accurate only from frequencies higher than 100 Hz. Conclusion was based on analysis of modal density. In this work, by comparing measured response and response calculated using statistical energy analysis, the practicable range of statistical energy analysis was found begun at lower frequencies, especially when first estimates of noise are needed in early design phase. The suitability of statistical energy analysis to early design phase was discussed by Plunt (2014). Comparison between results from measurements on board *Aranda* reported by Lamula (2015) and measured magnitude on one third octave bands, presented in figure 33, shows similar trend of response on both structures. Scale is different due to differences in structural properties and environment, such as dampening die more complex structure of *Aranda*, but similar trend illustrates similarities between structures and environmental conditions.

In tests reported by Lu et al. (1982) the finite element method was found out to be accurate to frequency of 100 Hz. Using Monte Carlo analysis, the accurate range was extended to 1000 Hz. In this work, on some locations the accurate range of single finite element analysis was extended considerably, but the analysis and frequency range was found out to be sensitive to the properties of the finite element model.

Calculations performed using statistical energy analysis and finite element method were extended beyond their limits, agreed by the literature. Finite element method provided accurate results, when water loading was correctly factored in low and mid frequencies. Statistical energy analysis provided usable results on whole frequency range.

9 Discussion

In the sea trials, measuring acceleration was found to be an error source, when measuring forced response on high loads. At two measurement locations, measurement of at least one directional component of acceleration response failed due accelerations exceeding limits of the accelerometer. Accelerometers were calibrated and fastened according to manufactures instructions. The instrumentation arrangement to measure force was developed for this work were unvalidated and could be a potential error source.

In a location nearest to shock impulse, measurement point #178, the measured acceleration to all three directions exceeded the range of accelerometers, thus the measurement on this location failed. On the other measurement location on the outside shell, measurement point #179, the measurements and response calculated using finite element method corresponded generally, but finite element method failed to calculate natural frequencies accurately. The velocity levels measured on the inside bulkhead, measurement location #113, did correspond to the velocity levels calculated using finite element method on two directions, but on the direction to the outside of the bulkhead the vibrational limit exceeded the limit of the accelerometer. Also in this location finite element method failed to calculate natural frequencies accurately. The error is caused by failure of wavelet method to predict the effect accurately when used together with finite element analysis. The finite element method did not provide accurate results on every location, and on every component. Accuracy of finite element analysis was highly dependent on the studied frequency band.

Lu et al. found (1982) the useful range of single finite element analysis be limited to lower frequencies, when compared against measurements of section of scale model of ship hull. In this thesis, the useful frequency range was extended, while found to be highly depended on propitiates of vibration, namely the wave length of vibration with the highest frequency. Also effects of water loading, omitted by Lu et al. were studied.

Comparison between velocity levels calculated using statistical energy analysis and measured magnitude of the vibration show close agreement on measurement point located on the outside shell, location #179, while omitting peaks on the whole studied frequency. Averaging behavior of statistical energy analysis is confirmed by the theory. In this thesis, statistical energy analysis was found to yield results close to those measured even in low frequencies. In low frequencies, according to theory statistical energy analysis would not be suitable.

This work confirmed the results of early studies of statistical energy analysis, applied to marine structure presented by Plunt and Lu et al. (1980b; 1982). Compared to these studies, in this work water loading was introduced into the model and confirmed against measurements. In this study useful range of statistical energy analysis, presented by Yayladere and Çalışka (2013) was extended to lower frequencies, by comparing results calculated using statical energy analysis and measurements on water loaded structure.

In this work finite element method and statistical energy analysis were to be found to supplement each other. Statistical energy analysis provided estimate of response on whole frequency range in major structural parts, while finite element method is more suitable to calculate accurate response to the level of small components in more defined frequency range.

For further study repeating these measurements using accelerometer with higher recording range would provide more validation material and failed measurements would more likely succeed. This research project will continue to repeating these calculations using *Aranda* of Finnish Environmental Institute as comparison. After *Aranda* is successfully introduced to VA One and methods are verified, tests are aimed to be repeated using Aranda at sea. First measurements will be carried out using known excitations and secondly using running engines as source. After that VA One is validated to use in modeling of structure-borne noise and sufficient knowledge is built in using VA One in marine environment together with ship product model.

An interesting and demanding further study would be creating a test method to verify transfer path analysis provided by VA One. It will be also useful to repeat these calculations using more accurate method to model the water loading of finite element method. To provide validation of statistical energy analysis in wider frequency range, these measurements should be repeated to frequencies at range of 30 kHz.

The choice of the method used in modeling of structure-borne sound modeling depends on frequency range and results needed. Finite element method is suitable to predict vibrational velocities at a relatively limited window of frequency range and model properties. Still, provided the right set of conditions, finite element method is capable to provide the accurate estimation of vibrational levels as demonstrated in this work. Statistical energy analysis is suitable to provide estimate at the approximate range of vibrational velocities when modal density is sufficiently large. It may be used from early design process to provide provide first estimates of noise levels of the ship as results of this thesis illustrate.

Statistical energy analysis is a potential tool to use design process, providing first estimates of vibrational levels when details of the structure are not finalized. In this work statistical energy analysis was found to work even in low frequencies for first estimates of vibrational levels. Statistical energy analysis can be used to calculate vibrational levels at the panels connecting to water, providing bases for calculating noise emissions to water. It can be also used to study transfer path to water, and to allow studying effects of noise control treatments.

Bibliography

Bertram, V. (2011) *Practical Ship Hydrodynamics*. 2nd edn. Oxford, United Kingdom: Butterworth-Heinemann.

Bies, D. and Hansen, C. (2003) *Engineering Noise Control*. 3rd edn. London, United Kingdom: Spon Press.

Biggs, J. (1994) *Introduction to Structural Dynamics*. New York, New York, USA: McGraw-Hill.

Blanchet, D. and Caillet, A. (2012) 'Predicting underwater sound radiation and directivity pattern of vibrating structures in deep and shallow water', in *Proceedings OF ISMA2012-USD2012*. *ISMA2012-USD2012*, Leuven, Belgium, pp. 4073–4082. Available at: http://www.isma-isaac.be/past/conf/isma2012/proceedings/papers/isma2012_0479.pdf (Accessed: 16 January 2015).

Borello, G. (2014) 'Virtual SEA Analysis of a Warship Classification', in. *10ème Congrès Français d'Acoustique*, Lyon, France. Available at: http://archivesic.ccsd.cnrs.fr/hal-00550544/document (Accessed: 15 January 2015).

Brunner, D., Junge, M. and Gaul, L. (2008) 'A comparison of FE–BE coupling schemes for large-scale problems with fluid–structure interaction', *International Journal for Numerical Methods in Engineering*, 77(5), pp. 664–688. doi: 10.1002/nme.2412.

Brunner, D., Junge, M., Wilken, M., Cabos, C. and Gaul, L. (2009) 'Vibro-acoustic simulations of ships by coupled fast BE-FE approaches', in *Proceedings of the IMAC-XXVII*. *IMAC XXVII*, Orlando, Florida, USA. Available at: http://sem-proceedings.com/27i/sem.org-IMAC-XXVII-Conf-s08p008-Vibro-acoustic-Simulations-Ships-by-Coupled-Fast-BE-FE-Approaches.pdf (Accessed: 5 December 2014).

Carcaterra, A. and Sestieri, A. (1997) 'Complex envelope displacement analysis: a quasi-static approach to vibrations', *Journal of Sound and Vibration*, 201(2), pp. 205–233. doi: 10.1006/jsvi.1996.0748.

Caresta, M. (2009) *Structural and acoustic responses of a submerged vessel*. PhD Thesis. University of New South Wales. Available at: http://handle.unsw.edu.au/1959.4/44404 (Accessed: 20 January 2015).

Caresta, M. and Kessissoglou, N. J. (2010) 'Acoustic signature of a submarine hull under harmonic excitation', *Applied Acoustics*, 71(1), pp. 17–31. doi: 10.1016/j.apacoust.2009.07.008.

Carlton, J. and Vlašić, D. (2005) ‘Ship vibration and noise: Some topical aspects’, in *Lloyd’s Register Technical Papers*. *1st International Ship Noise and Vibration Conference*, London, United Kingdom. Available at: http://www.shipsuperintendent.com/Welcome/L160.pdf (Accessed: 13 November 2015).

Cicirello, A., Langley, R., Kovalevsky, L. and Woodhouse, J. (2012) ‘The Hybrid Finite Element/Statistical Energy Analysis method’, in *Methodologies for Mid-Frequency Analysis in Vibration and Acoustics*. Heverlee, Belgium: Katholieke Universiteit Leuven, pp. 233–262.

Clancy, T. (1987) *Red Storm Rising*. New York, New York, USA: Penguin Group.

Collier, R. (1997) ‘Ship and Platform Noise, Propeller Noise’, in Crocker, M. (ed.) *Encyclopedia of acoustics. Vol. 1, General linear acoustics, nonlinear acoustics and cavitation, aeroacoustics and atmospheric sound, underwater sound*. New York, New York, USA: Wiley, pp. 521–537.

Cook, R., Malkus, D. and Plesha, M. (1989) *Concepts and applications of finite element analysis*. New York, New York, USA: Wiley,.

COSMIC (1981) *NASTRAN Theoretical Manual*. Athens, Georgia, USA: The University of Georgia Computer Services Annex. Available at: http://ntrs.nasa.gov/archive/nasa/casi.ntrs.nasa.gov/19840010609.pdf (Accessed: 14 March 2016).

Cotoni, V., Shorter, P. and Langley, R. (2007) ‘Numerical and experimental validation of a hybrid finite element-statistical energy analysis method’, *The Journal of the Acoustical Society of America*, 122(1), pp. 259–270. doi: 10.1121/1.2739420.

Cremer, L., Heckl, M. and Petersson, B. (2005) *Structure-borne sound*. 3rd edn. Berlin, Germany: Springer.

Cuschieri, J. M. and Sun, J. C. (1994) ‘Use of Statistical Energy Analysis for Rotating Machinery, Part III: Experimental Verification With Machine on Foundation’, *Journal of Sound and Vibration*, 170(2), pp. 203–214. doi: 10.1006/jsvi.1994.1056.

Deckers, E., Atak, O., Coox, L., D’Amico, R., Devriendt, H., Jonckheere, S., Koo, K., Pluymers, B., Vandepitte, D. and Desmet, W. (2014) ‘The wave based method: An overview of 15 years of research.’, *Wave Motion*, 51(4), pp. 550–565. doi: 10.1016/j.wavemoti.2013.12.003.

Desmet, W. (1998) *A wave based prediction technique for coupled vibro-acoustic analysis*. PhD Thesis. Katholieke Universiteit Leuven. Available at: https://www.mech.kuleuven.be/en/doctorates/desmet.pdf (Accessed: 5 December 2014).

Desmet, W., Pluymers, B. and Atak, O. (2012) *Methodologies for Mid-Frequency Analysis in Vibration and Acoustics*. Heverlee, Belgium: Katholieke Universiteit Leuven. Available at: http://www.midfrequency.org/documents/mid-frequency-final-book (Accessed: 1 December 2015).

Dixon, J. C. (2007) *The Shock Absorber Handbook*. Chichester, United Kingdom: John Wiley & Sons, Ltd.

ESI Group (2003) 'ESI Group Unveils At MICAD the Most Comprehensive Vibro-Acoustic Simulation Solution'. Available at: http://news.thomasnet.com/fullstory/software-performs-vibro-acoustic-simulation-21331 (Accessed: 26 May 2015).

ESI Group (2013) 'The Story of ESI'. Available at: https://www.esi-group.com/sites/default/files/resource/brochure_flyer/10/historical_summary.pdf (Accessed: 26 May 2015).

ESI Group (2015) 'Va One User Manual'.

Fahy, F. J. (2000) *Foundations of Engineering Acoustics*. Oxford, United Kingdom: Academic Press.

Fahy, F. J. and Gardonio, P. (2007) *Sound and Structural Vibration : Radiation, Transmission and Response*. 2nd edn. Jordan Hill, United Kingdom: Academic Press.

Fischer, R. and Collier, R. D. (2007) 'Noise Prediction and Prevention on Ships', in Crocker, M. J. (ed.) *Handbook of Noise and Vibration Control*. Hoboken, New Jersey, USA: John Wiley & Sons, Inc., pp. 1216–1232. Available at: http://doi.wiley.com/10.1002/9780470209707.ch101 (Accessed: 9 February 2015).

Fishman, G. (2008) *Monte Carlo: concepts, algorithms, and applications*. 7th edn. New York, New York, USA: Springer.

Franklin, M., Suckow, S. and Weisbroth, C. (eds) (1995) 'Water, air and ice', in *Seawater (Second Edition)*. Oxford: Butterworth-Heinemann, pp. 4–13.

Granda Design Limited (2015) *CES EduPack 2015*. Available at: http://www.grantadesign.com/education/ (Accessed: 3 March 2016).

Henry, A. (2015) 'VA One Training'. Munich, Germany.

Heron, K. H. (1997) 'Predictive statistical energy analysis and equally spaced point connections', in *Proceedings of the fifth international congress on sound and vibration*. *Fifth international congress on sound and vibration*, Adelaide, Australia. Available at: http://www.acoustics.asn.au/conference_proceedings/ICSVS-1997/pdf/scan/sv970318.pdf (Accessed: 23 February 2016).

Homm, A., Ehrlich, J., Peine, H. and Wiesner, H. (2003) ‘Experimental and numerical investigation of a complex submerged structure. Part I: Modal analysis’, *ACTA ACUSTICA UNITED WITH ACUSTICA*, 89(1), pp. 61–70.

Hynnä, P., Klinge, P. and Vuoksinen, J. (1995) ‘Prediction of structure-borne sound transmission in large welded ship structures using statistical energy analysis’, *Journal of Sound and Vibration*, 180(4), pp. 583–607. doi: 10.1006/jsvi.1995.0101.

International Maritime Organization (2014) ‘Guidelines for the Reduction of Underwater Noise’. International Maritime Organization. Available at: http://docs.nrdc.org/water/wat_14050501.asp (Accessed: 2 October 2015).

Jaouen, L. (2011) *Narrow bands to one-third octave bands representation*. Available at: http://apmr.matelys.com/Standards/OctaveBands.html (Accessed: 3 March 2016).

Lamula, L. (2015) *Taajuusvastemittaukset Arandalla*. Measurement report 107556/ Aranda15. Tampere, Finland: VTT.

Langley, R. (1994) ‘Elastic Wave Transmission Coefficients and Coupling Loss Factors for Structural Junctions Between Curved Panels’, *Journal of Sound and Vibration*, 169(3), pp. 297–317. doi: 10.1006/jsvi.1994.1020.

Langley, R. (2007) ‘Numerical evaluation of the acoustic radiation from planar structures with general baffle conditions using wavelets’, *The Journal of the Acoustical Society of America*, 121(2), p. 766. doi: 10.1121/1.2405125.

Langley, R. and Heron, K. (1990) ‘Elastic wave transmission through plate/beam junctions’, *Journal of Sound and Vibration*, 143(2), pp. 241–253. doi: 10.1016/0022-460X(90)90953-W.

Langley, R. and Shorter, P. (2002) ‘Diffuse wavefields in cylindrical coordinates’, *The Journal of the Acoustical Society of America*, 112(4), p. 1465. doi: 10.1121/1.1502895.

Langley, R. and Shorter, P. (2003) ‘The wave transmission coefficients and coupling loss factors of point connected structures’, *The Journal of the Acoustical Society of America*, 113(4), pp. 1947–1964. doi: 10.1121/1.1515791.

Leissa, A. (1969) *Vibration of plates*. NASA-SP-160. Washington, District of Columbia , USA: NASA, p. 362. Available at: http://ntrs.nasa.gov/search.jsp?R=19700009156.

Leppington, F., Broadbent, E. and Heron, K. (1982) ‘The Acoustic Radiation Efficiency of Rectangular Panels’, *Proceedings of the Royal Society of London. Series A, Mathematical and Physical Sciences*, 382(1783), pp. 245–271.

Linjama, J. (1991) ‘Äänen ja tärinän eteneminen rakennusrungossa’, *Rakenteiden mekaniikka*, 24(1), pp. 45–54.

Lin, T., Pan, J., O'Shea, P. and Mechefske, C. (2009) 'A study of vibration and vibration control of ship structures', *Marine Structures*, 22(4), pp. 730–743. doi: 10.1016/j.marstruc.2009.06.004.

Lloyd's Register (2015) 'Guidance Notes General Overview of Ship Structural Vibration Problems'. Available at: https://www.cdlive.lr.org/information/documents%5CLRGuidance%5CGuidance%20Notes_General%20Overview%20of%20Ship%20Structural%20Vibration%20Problems_COMPLETE.pdf (Accessed: 3 March 2016).

Lucas, G. (2008) *Vibrational characteristics of structures with uncertainty*. PhD Thesis. University of New South Wales. Available at: http://handle.unsw.edu.au/1959.4/41274 (Accessed: 20 January 2015).

Lu, L., Hawkins, W., Downard, D. and DeJond, R. (1982) 'Comparison of Statistical Energy Analysis and Finite Element Analysis Vibration Prediction with Experimental Results', in *The Shock and Vibration Bulletin*. *Symposium on Shock and Vibration*, Danvers, Massachusetts, USA: The Shock and Vibration Information Center (4), pp. 145–153. Available at: http://www.dtic.mil/dtic/tr/fulltext/u2/a134455.pdf (Accessed: 17 February 2016).

Lyon, R. and DeJong, R. (1994) *Theory and Applications of Statical Energy Analysis*. 2nd edn. Newton, Massachusetts, USA: Butterworth-Heinemann.

Mansfield, M. and O'Sullivan, C. (2011) *Understanding physics*. 2nd edn. Hoboken, New Jersey, USA: Wiley.

National Land Survey of Finland (2015) *Paikkatietoikkuna*. Available at: http://www.paikkatietoikkuna.fi (Accessed: 21 March 2016).

Pirovsky, C., Stefanov, S., Draganchev, H. and Valchev, S. (2012) 'Numerical modeling of ship's vibrations and model validation by full-scale dynamic test', in *Proceedings of ISMA 2012 International Conference on Noise and Vibration Engineering*. *ISMA2012 International Conference on Noise and Vibration Engineering*, Leuven, Belgium, pp. 3223–3237.

Plunt, J. (1980a) *Methods for Predicting Noise Levels in Ships, Part I*. PhD Thesis. Kalmers University of Technology.

Plunt, J. (1980b) *Methods for Predicting Noise Levels in Ships, Part II*. PhD Thesis. Kalmers University of Technology.

Plunt, J. (2014) 'Examples of early use of Statistical Energy Analysis (SEA) for concept development evaluation', in *Proceedings of the 9th International Conference on Structural Dynamics, EURODYN 2014*. *9th International Conference on Structural*

Dynamics, Porto, Portugal. Available at: http://paginas.fe.up.pt/~eurodyn2014/CD/program.html.

Pluymers, B. (2006) *Wave based modeling methods for steady-state vibro-acoustics*. PhD Thesis. Katholieke Universiteit Leuven. Available at: people.mech.kuleuven.be/~bpluymer/docs/thesis_bpluymers.pdf (Accessed: 30 January 2015).

Protection of the Arctic Marine Environment Working Group (2009) *Arctic Marine Shipping Assessment 2009*. Monograph. Arctic Council. Available at: http://library.arcticportal.org/1400/ (Accessed: 2 October 2015).

Rabbiolo, G., Bernhard, R. and Milner, F. (2004) 'Definition of a high-frequency threshold for plates and acoustical spaces', *Journal of Sound and Vibration*, 277(4-5), pp. 647–667. doi: 10.1016/j.jsv.2003.09.015.

Ross, D. (1987) *Mechanics of underwater noise*. Los Altos, California, USA: Peninsula Publishing.

Santaoja, K. (2009) *Lujuusoppi I*. 2nd edn. Helsinki, Finland: Otamedia.

Sharqawy, M., Lienhard, J. and Zubair, S. (2010) 'Thermophysical properties of seawater: a review of existing correlations and data', *Desalination and Water Treatment*, 16(1-3), pp. 354–380. doi: 10.5004/dwt.2010.1079.

Shorter, P. and Langley, R. (2005) 'Vibro-acoustic analysis of complex systems', *Journal of Sound and Vibration*, 288(3), pp. 669–699. doi: 10.1016/j.jsv.2005.07.010.

Soedel, W. (2004) *Vibrations of shells and plates*. 3rd edn. New York, New York, USA: Dekker (Mechanical engineering, 177).

Soize, C., Desanti, A. and David, J.-M. (1992) 'Numerical methods in elastoacoustic for low and medium frequency ranges', *La Recherche Aerospatiale (English edition)*, 5, pp. 25–44.

Tratch, J. (1985) *Vibration transmission through machinery foundation and ship bottom structure*. M. Sci Thesis. Massachusetts Institute of Technology. Available at: http://hdl.handle.net/1721.1/15216 (Accessed: 27 January 2015).

Wachulec, M., Kirkegaard, P. and Nielsen, S. (2000) 'Methods of estimation of structure borne noise in structures-Review', *Structural Dynamics*, 20. Available at: http://www.wind.civil.aau.dk/dynpaper/paper20.pdf (Accessed: 4 February 2015).

World Weather Online (2016) *Pargas Historical Weather, Finland*. Available at: http://www.worldweatheronline.com/pargas-weather-history/southern-finland/fi.aspx (Accessed: 3 February 2016).

Yayladere, B. and Çalışkan, M. (2013) ‘Prediction of noise levels within a submerged vessel by statistical energy analysis’, in. *20th International Congress on Sound and Vibration*, Bangkok, Thailand. Available at: http://www.mezzostudyo.com/medya/pdf/3271389883293.pdf (Accessed: 20 January 2015).

Zienkiewicz, O., Taylor, R., Zhu, J. and Taylor, R. (2013) *The Finite Element Method : Its Basis and Fundamentals*. Amsterdam, Netherlands: Elsevier Butterworth-Heinemann.

Zuckerwar, A. (1997) ‘Speed of Sound in Fluids’, in Crocker, M. (ed.) *Encyclopedia of acoustics. Vol. 1, General linear acoustics, nonlinear acoustics and cavitation, aeroacoustics and atmospheric sound, underwater sound*. New York, New York, USA: Wiley.